AD-A072 296 AIR FORCE FLIGHT DYNAMICS LAB WRIGHT-PATTERSON AFB OH F/G 16/3
OPTIMUM SHAPE FOR TRANSPIRATION-COOLED NOSETIP OF A RE-ENTRY VE--ETC(U)
NOV 78 K E YELMGREN

UNCLASSIFIED AFFDL-TR-78-147 NL

1 OF 1
AD
A072296

END
DATE
FILMED
9-79
DDC

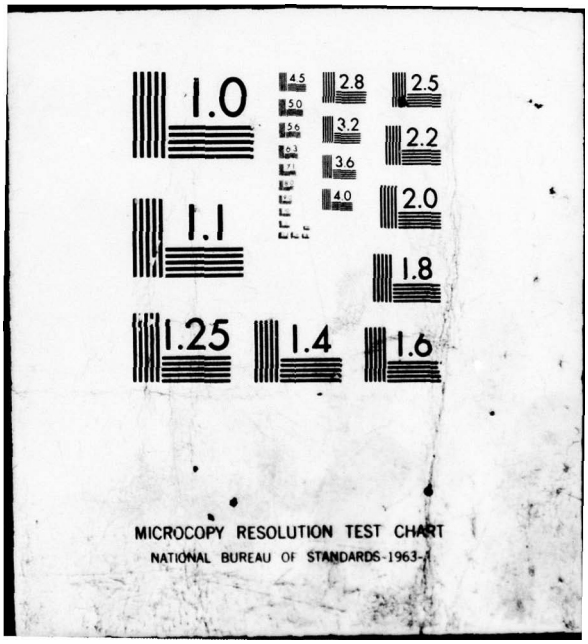
1.0
1.1
1.25
1.4
1.6
1.8
2.0
2.2
2.5
2.8
3.2
3.6
4.0
4.5
5.0
5.6
6.3
MICROCOPY RESOLUTION TEST CHART
NATIONAL BUREAU OF STANDARDS-1963-A

AFFDL-TR-78-147

LEVEL II

OPTIMUM SHAPE FOR TRANSPIRATION-COOLED NOSETIP OF A RE-ENTRY VEHICLE

Kevin E. Yelmgren, Captain, USAF
Thermomechanics Branch
Aeromechanics Division

November 1978

TECHNICAL REPORT AFFDL-TR-78-147

Final Report for Period October 1974 - June 1978

Approved for public release; distribution unlimited.

AIR FORCE FLIGHT DYNAMICS LABORATORY
AIR FORCE WRIGHT AERONAUTICAL LABORATORIES
AIR FORCE SYSTEMS COMMAND
WRIGHT-PATTERSON AIR FORCE BASE, OHIO 45433

NOTICE

When Government drawings, specifications, or other data are used for any purpose other than in connection with a definitely related Government procurement operation, the United States Government thereby incurs no responsibility nor any obligation whatsoever; and the fact that the government may have formulated, furnished, or in any way supplied the said drawings, specifications, or other data, is not to be regarded by implication or otherwise as in any manner licensing the holder or any other person or corporation, or conveying any rights or permission to manufacture, use, or sell any patented invention that may in any way be related thereto.

This report has been reviewed by the Information Office (OI) and is releasable to the National Technical Information Service (NTIS). At NTIS, it will be available to the general public, including foreign nations.

This technical report has been reviewed and is approved for publication.

Kevin E. Yelmgren

KEVIN E. YELMGREN, Captain, USAF
Project Engineer

J. Christopher Boison

J. CHRISTOPHER BOISON
Chief, Thermomechanics Branch
Aeromechanics Division

FOR THE COMMANDER

Donald J. Harney

DONALD J. HARNEY
Assistant for Experimental Simulation
Aeromechanics Division
AF Flight Dynamics Laboratory

"If your address has changed, if you wish to be removed from our mailing list, or if the addressee is no longer employed by your organization please notify AFFDL/FXE ,W-PAFB, OH 45433 to help us maintain a current mailing list".

Copies of this report should not be returned unless return is required by security considerations, contractual obligations, or notice on a specific document.

AIR FORCE/56780/26 July 1979 — 150

SECURITY CLASSIFICATION OF THIS PAGE (When Data Entered)

REPORT DOCUMENTATION PAGE

READ INSTRUCTIONS BEFORE COMPLETING FORM

1. REPORT NUMBER: AFFDL-TR-78-147	2. GOVT ACCESSION NO.
3. RECIPIENT'S CATALOG NUMBER	
4. TITLE (and Subtitle): OPTIMUM SHAPE FOR TRANSPIRATION-COOLED NOSETIP OF A RE-ENTRY VEHICLE	5. TYPE OF REPORT & PERIOD COVERED: Final Report, Oct 74 – Jun 78
6. PERFORMING ORG. REPORT NUMBER	
7. AUTHOR(s): Kevin E. Yelmgren, Captain, USAF	8. CONTRACT OR GRANT NUMBER(s)
9. PERFORMING ORGANIZATION NAME AND ADDRESS: Air Force Flight Dynamics Laboratory (FXE), Air Force Wright Aeronautical Laboratories, Wright-Patterson AFB, Ohio 45433	10. PROGRAM ELEMENT, PROJECT, TASK AREA & WORK UNIT NUMBERS: Project 2404, Task 240404, Work Unit 24040401
11. CONTROLLING OFFICE NAME AND ADDRESS: Air Force Flight Dynamics Laboratory (FX), Air Force Wright Aeronautical Laboratories, Wright-Patterson AFB, Ohio 45433	12. REPORT DATE: Nov 78
	13. NUMBER OF PAGES: 93
14. MONITORING AGENCY NAME & ADDRESS (if different from Controlling Office): 93 p.	15. SECURITY CLASS. (of this report): Unclassified
	15a. DECLASSIFICATION/DOWNGRADING SCHEDULE

16. DISTRIBUTION STATEMENT (of this Report)

Approved for public release; distribution unlimited.

17. DISTRIBUTION STATEMENT (of the abstract entered in Block 20, if different from Report)

18. SUPPLEMENTARY NOTES

19. KEY WORDS (Continue on reverse side if necessary and identify by block number)

Transpiration-Cooled Nose Tip
Reentry Aerodynamic Heating
Optimum Nose Shape for Reentry Vehicles

20. ABSTRACT (Continue on reverse side if necessary and identify by block number)

The variations of parameters method was used to determine the optimum nose shape for a reentry vehicle having a transpiration-cooled nosetip (TCNT). Three families of nose shapes were considered - The oblate ellipsoid, the flat face - round shoulder, and the spherical arc - round shoulder. These families are bounded by the flat face - sharp corner at one extreme and the hemisphere at the other extreme. The amount of coolant required by each nose shape during reentry was determined by using a high speed computer to

(over)

DD FORM 1 JAN 73 1473 EDITION OF 1 NOV 65 IS OBSOLETE

012 070

SECURITY CLASSIFICATION OF THIS PAGE (When Data Entered)

20. ABSTRACT (Continued)

couple the aerodynamic equations with the trajectory equations. The optimum shape is the shape which requires the least amount of coolant for reentry. The flat face - sharp corner shape was found to require the least amount of coolant, about sixty percent less water than the hemisphere. Although the time to impact is longer for the flat face, the smaller surface area and lower heating intensity more than offsets the increased reentry time. The possibility of an optimum flat face height was also investigated; no face height was found that minimized the total heating to the vehicle during reentry.

FOREWORD

This technical report was written by Capt Kevin E. Yelmgren of the Thermomechanics Branch, Aeromechanics Division, Air Force Flight Dynamics Laboratory, Wright-Patterson Air Force Base, Ohio 45433. The work was accomplished under Work Unit Number 24040401, "Active Cooling Concepts."

This report covers the period from October 1974 to June 1978. It was submitted for review in September 1978.

TABLE OF CONTENTS

TABLE OF CONTENTS (CONCLUDED)

LIST OF ILLUSTRATIONS

LIST OF TABLES

NOMENCLATURE

a	Nose base radius (in)
a_{SL}, a_{02}	Speed of sound, (ft/sec), sea level and stagnation value
a_d	dT/dh_G
a_s	Constant defined by Equation 50b
A_v	Constant defined by Equation 53a
A_μ	Constant defined by Equation 88d
A_0, A_1, A_2	Constants defined by Equations 73a, b, c
a_1, a_2, a_3	Constants defined by Equations 105c, d, e
A_B	Base area (ft^2)
b	Minor axis of ellipse, Sketch 1 intercept of straight line for shock stand-off (in)
B_v	Constant defined as (20/9) $\bar{R}_{sh}$ Equation 53b
B_2, B_4	Equations 54a and 54b
b_1, b_2	Constants, Equations 84c and 84d
B	Blowing parameter, $\dot{m}/\rho_e u_e\ St_o$
B_s	Constant used in Equation 47
c	Semi focal length of ellipse (in)
C_0, C_1, C_2	Constants defined by Equations 44b, 44c, and 46a
C_D	Drag coefficient
C_1, C_2, C_4, C_6, C_7, C_8	Constants defined by Equations 56a thru 56f
C_3	Constant defined by Equation 60
C_p	Specific heat of air at constant pressure (0.23991 BTU/lbm°R)
C_f	Skin friction coefficient
C^*	Rubesin Coefficient, $\rho^*\mu^*/\rho_e\mu_e$
d	Diameter (in)
d_1, d_2	Constants, Equations 57a and 57b

NOMENCLATURE (CONTINUED)

D_p	Pressure drag (lbf)
D_{sf}	Skin frinction drag (lbf)
D_B	Base drag (lbf)
D_T	Total drag, $\gamma_{DP} + D_{sf} + D_B$ (lb_f)
DC	Diffusion corrections, Equation 100
e_1, e_2	Constants defined by Equations 39a, 39b
F(s)	Heat transfer function, Equation 95b
g	Gravitational acceleration (ft/sec^2)
g_c	32.174 ($ft\text{-}lbm/sec^2\text{-}lbf$)
h	Local enthalpy (BTU/lbm)
h_g	Geopotential altitude (ft)
h_G	Geometric altitude, from earth's surface (ft)
h_a	Absolute altitude from earth's center (ft)
h_b	Base altitude for atmospheric calculations (ft)
H	Total enthalpy (BTU/lbm)
h_1	Enthalpy constant in density calculation (BTU/lbm)
h_D	Enthalpy of dissociation (BTU/lbm)
ΔH_c	Total enthalpy rise of coolant. For water assumed to be 1150 BTU/lbm.
$\overline{H}$	Constant for $\dot{m}$ calculation, Equation 105f
J	778.161 (ft-lbf)/BTU
J_p	Pressure gradient at sonic point; $(d\overline{p}/d\theta)$ Equation 62a
J_s	Velocity gradient, Equation 87b
k_s	Constant defined by Equation 50a
k	Density ratio across shock, ρ_∞/ρ_2

NOMENCLATURE (CONTINUED)

K_v	Constant defined by Equation 54c
K_p	Constant defined by Equation 62b
K_1	Constant defined by Equation 79c
L	Length of cone (in)
M	Mach number
m_{SA}	Slope of straight line, Equation 46c
M_f	Mangler factor in skin friction equation, Equation 97c
$\dot{m}$	Coolant mass flux (lbm/ft^2-sec)
m	Mass of vehicle (slugs)
$\dot{M}$	Coolant flow rate (lbm/sec)
η	constant defined by Equation 50c
Nu	Nusselt number
P, Pa	Pressure (lbf/ft^2); atm respectively)
P	Nondimensional pressure, P/P_{o_2}
P_{o_2}	Stagnation pressure on body (lbf/ft^2)
P_1, P_2, P_3	Constants defined by Equations 55b - 55d
$\tilde{P}$	Nondimensional pressure, Equation 79b
Pr	Prandtl number
$\dot{q}$	Heat flux (BTU/ft^2-sec)
q_∞	Dynamic pressure (lbf/ft^2)
r	Axial distances, Sketch 2 (in)
r_c	Radius of corner for flat face nose and spherical arc nose, Sketches 3 and 4 (in)
r_f	Recovery factor
R	Gas Constant, 53.35 ft/°R

NOMENCLATURE (CONTINUED)

R_N	Radius of nose for spherical arc (in)
R_B	Vehicle base radius, Sketch 6 (in)
R_{er}	Radius of earth; 20,855,531.5 ft
R_{s_o}	Shock radius of curvature at stagnation point (in)
$\bar{R}_{s_o}$	Nondimensional shock radius of curvature (R_{s_o}/a)
Re_s	Reynolds number based on arc length
Re_θ	Reynolds number based on momentum thickness
s	Arc length measured from stagnation point (in)
s_o	Shock stand-off distance (in)
S_L	Arc length over which velocity varies linearly (in)
St	Stanton number
S	Surface area, ft^2
T	Temperature, °R
T_1	Temperature for atmospheric calculation °R
t	Time (sec)
Δt	Time step for trajectory calculations (sec)
u	Velocity (ft/sec)
u_L	Velocity value at end of linear region (ft/sec)
V_∞	Velocity of re-entry vehicle (ft/sec)
W	Specific heat ratio for water vapor to air. Assumed to be 1.86
wt	Weight of reentry vehicle (lbs)

NOMENCLATURE (CONTINUED)

X	Axial coordinate, Sketch 1 (in)
$\tilde{X}$	Nondimensional axial coordinate, Equation 79a
X_J	Axial distance from nose tip to cone junction (in)
X_K	Axial distance measured from shoulder point (in)
X_{ISH}	Axial distance from nose tip to shoulder, Sketch 1 (in)
X	Trajectory range point of reentry (ft)
X^1	Axial distance measured from X_J Sketch 1 (in)
X_ρ	Constant defined by Equation 89b
y	Radial distance from centerline, Sketch 1 (in)
z	Axial distance, Sketch 2 (in)
Z	$(a/R_N)^{-1}$
Z_A	Constant defined by Equation 126b or c
Z_k	Constant defined by Equation 126d
Z_m	Constant defined by Equation 126e
Z_t	Constant defined by Equation 124
α	Constant defined by Equation 126a
β	Trajectory constant, $WT/C_D A_B$ (lb/ft^2)
γ	Ratio of specific heats
γ_E	Reentry angle (degrees)
$\dot{\gamma}$	Rate of change of reentry angle (degree/sec)
Δ	Spherical arc-sharp corner axial distance to shoulder (in)
δ_1	Base pressure ratio (P_1/P_{SL}) for atmospheric calculation
Δ_*	Value of Δ for sonic point on corner (in)
$\tilde{\Delta}$	Defined by Equation 44d

NOMENCLATURE (CONCLUDED)

$\tilde{\Delta}_{MP}$	Match point location, defined by Equation 45
δ^{**}	Momentum thickness
ε_T	Constant in skin friction equation, defined by Equation 97b
η	Elliptic coordinate, Sketch 2
θ	Angle between X axis and tangent to body, Sketch 1 (degrees)
K	Constant defined by Equation 6b
K_S	Constant defined by Equation 88c
$\overline{\lambda}$	Constant defined by Equation 54d
μ	Viscosity (slug/ft-sec)
ξ	Elliptic coordinate, Sketch 2
ξ_B	Elliptic coordinate for body
$\overline{\xi}_s$	Defined by Equation 55a
π	3.1415962
ρ, ρ_1	Density (slugs/ft^3)
ρ_∞	Freestream density (slugs/ft^3)
ρ_2	Density behind shock (slugs/ft^3)
σ_1	Base density ratio $\frac{\rho_1}{\rho_{SL}}$ for atmospheric calculations
τ	Skin friction (lbf/ft^2)
ϕ	Angle between axis and perpendicular to body, Sketch 3 (degrees)
$\dot{\phi}$	Time rate of change of reentry angle from earth's center (degrees/sec)
ω	Constant defined by Equation 6b

SUBSCRIPTS

B	Body; base of vehicle
c	Cone aft body
e	Boundary layer edge value; oblate ellipsoid value
E	Initial reentry condition
f	Flat face-sharp corner value
h	Hemispherical value
I	Intersection of nose with corner, Sketch 3
ISH	Shoulder point of nose, Sketch 1
J	Junction of nose with aft body, Sketch 1
MIN	Minimum value from Krasnov's universal curve
NB	No blowing value
PM	Prandtl-Meyer value
r	Recovery value
SA	Spherical arc-sharp corner value
SL	Sea level value
w	Wall value
○	Location of corner, Sketch 3; no blowing value; stagnation value
0.5	Oblate ellipsoid value, b/a=0.5
∞	Freestream condition

SUPERSCRIPTS

*	Sonic point value; reference enthalpy value

SECTION I

INTRODUCTION

The active cooling of re-entry nose tips may be the only practical method of maintaining a shape stable nose in a severe weather environment. The coolant provides protection from the thermal and particle environments, and the degree of protection depends on how effectively the available coolant is used. The transpiration-cooled nose tip (TCNT) is one means of actively cooling the nose tip. By minimizing the coolant necessary for thermal protection, more coolant is available for particle protection. One of the options available for reducing the amount of coolant for thermal protection is to optimize the external shape of the nose tip. The objective of this investigation is to determine the external shape of a TCNT that requires the minimum amount of coolant over a re-entry trajectory.

The general problem of minimizing the aerodynamic heating to a hypersonic vehicle has been considered by various authors (References 1, 2, 3, and 4). All of these studies used the calculus of variations method and assumed a modified Newtonian pressure distribution, either completely laminar or completely turbulent flow, and constant freestream conditions. The specific case of the TCNT was considered by Baker and Kramer (Reference 5). They also assumed a modified Newtonian pressure distribution, and either completely laminar or completely turbulent flow. Instead of constant freestream conditions, however, their trajectory parameter beta, WT/C_DA_B, was assumed to be a constant. All but one of these studies concluded that the flat face - sharp corner shape minimized the total heat load to the vehicle, and that for a given fineness ratio there was an optimum flat face height. Furey's (Reference 3) results differed in that the flat face had a small "bubble" at the stagnation point. Hull (Reference 6) has pointed out the mathematical restrictions that result from using the above assumptions with the calculus of variations method. These restrictions make the results in the literature mathematically questionable. Baker and Kramer did take Hull's results into

consideration in their investigation but they assumed that the flat face nose was the optimum shape without ever proving it.

The results in the literature may also be questioned from a practical viewpoint. The modified Newtonian pressure distribution is of course accurate for the hemisphere but not for the blunter shapes such as the flat face. The boundary layer flow over the vehicle is usually a combination of both laminar and turbulent and, as turbulent flow is associated with much higher heating, the effect of the nose shape on transition is an important factor. The freestream conditions, as well as beta, vary throughout the trajectory. Assuming that either of these is a constant removes the effect of the nose shape on the trajectory time which is another factor effecting the total coolant required. In view of the above, it was decided to reconsider the optimum TCNT problem and use the variation of parameters method rather than the calculus of variations method. The variation of parameters method requires the calculation of the total coolant needed by a given nose shape during reentry. The optimum shape is the shape requiring the least amount of coolant. This method allows the optimum shape to be more realistically determined as the assumptions mentioned above do not have to be made.

As the optimum shape is determined by comparing the amount of coolant required by one shape with that required by another shape, only relative accuracy is required in the calculations. The simpler empirical methods available in the literature were used to calculate the aerodynamic heating and drag. Some of these methods are valid only for hypersonic speeds, hence this investigation is restricted to impact Mach numbers greater than four. Three different families of nose shapes were considered - the oblate ellipsoid, the flat face - round shoulder, and the spherical arc - round shoulder. These families are bounded by the flat face - sharp corner at one extreme and the hemisphere at the other extreme. A ten-degree half-angle cone was used as the aft body for all three shapes. The transpirant, water, was assumed to cool only the nose as the aft body heating is usually handled by an ablative material. The wall temperature of the nose was assumed to be 2000°R. At each

altitude the coolant flow and total drag on the vehicle were calculated. The trajectory equations were used to calculate the next altitude, velocity, reentry angle and range for a given time step. A time step was chosen such that the drag coefficient was nearly constant. The coolant used over the entire trajectory was determined by numerically integrating the amount of coolant used at each time step.

The geometric considerations are presented in Section II. The inviscid analysis is covered in Section III. This includes the shock stand - off distance as well as the properties behind the shock and at the body stagnation point. The viscous calculations are discussed in Section IV and the trajectory in Section V. The validation of the computer results is presented in Section VI. In this section, the computer program results are compared to data in the literature or values obtained from hand calculation. In Section VII the results of this investigation are discussed, and in Section VIII, the conclusions are presented.

SECTION II

VEHICLE GEOMETRY

The equations used for calculating the various geometries are summarized in this section. The independent variable for the nose is y, while the arc length, s, is used as the independent variable on the aft body.

1. OBLATE ELLIPSOID

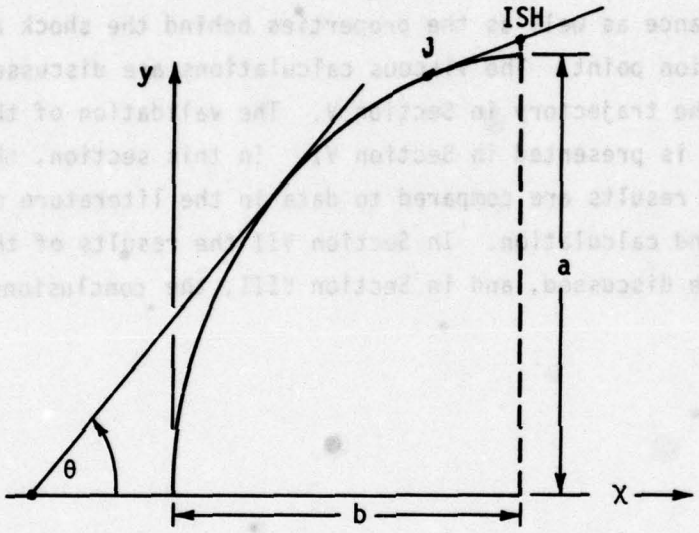

Sketch 1. Oblate Ellipsoid

The equation for an ellipse in the coordinate system shown above is

$$\frac{(x - b)^2}{b^2} + \frac{y^2}{a^2} = 1 \qquad (1)$$

The intersection of the nose with the cone aft body occurs when $\theta = \theta_c$. The coordinates of this junction are

$$x_J = b - \frac{b^2}{a} \frac{\tan \theta_c}{\sqrt{1 + \frac{b^2}{a^2} \tan^2 \theta_c}} \qquad (2a)$$

$$y_J = \frac{a}{\sqrt{1 + \frac{b^2}{a^2} \tan^2 \theta_c}} \tag{2b}$$

The shoulder point location, ISH, is given by

$$x_{ISH} = b \tag{3a}$$

$$y_{ISH} = y_J + (b - x_J) \tan \theta_c \tag{3b}$$

The arc length along an ellipse can be conveniently expressed in terms of the elliptic coordinates (ξ,η).

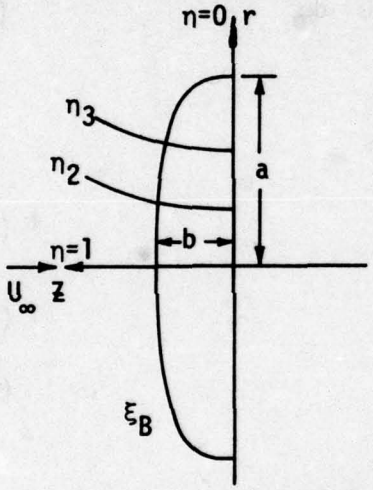

Sketch 2. Elliptic Coordinates

$$c^2 = a^2 - b^2 \tag{4}$$

$$r^2/c^2 = (1 + \xi^2)(1 - \eta^2) \tag{5a}$$

$$z/c = \xi\eta \tag{5b}$$

$$\xi_B = b/c \tag{5c}$$

then

$$\frac{s}{c} = \int_1^{\eta} \sqrt{\frac{\eta^2 + \xi_B^2}{1 - \eta^2}}\, d\eta \tag{6a}$$

$$\text{If } \eta = \cos\omega, \text{ and } \xi_B^2 = \left(\frac{1 - K^2}{K^2}\right), \tag{6b}$$

then

$$\frac{s}{a} = \int_{\cos\omega}^{0} \sqrt{1 - K^2 \sin^2 \omega}\, d\omega \tag{7}$$

This is an elliptic integral of the second kind.

Using y as the independent variable, values of x, θ, η, are given by

$$\chi = b\left\{1 - \sqrt{1 - y^2/a^2}\right\} \tag{8a}$$

$$\theta = \tan^{-1}\left\{\frac{a}{b}\sqrt{\frac{a^2}{y^2} - 1}\right\} \tag{8b}$$

$$\eta = \frac{(b/a)\tan\theta}{\sqrt{1 + (\frac{b}{a})^2 \tan^2\theta}} = \frac{y}{a}\sqrt{\frac{a^2}{y^2} - 1} \tag{8c}$$

$$\frac{s}{a} = \int_{\cos\omega}^{o} \sqrt{1 - K^2 \sin^2\omega}\ d\omega \tag{8d}$$

For values of y between y_J and y_{ISH}

$$\chi = \chi_J + (y - y_J)/\tan\theta_c \tag{9a}$$

$$s = s_J + (y - y_J)/\sin\theta_c \tag{9b}$$

$$\theta = \theta_c \tag{9c}$$

2. FLAT FACE - ROUND SHOULDER

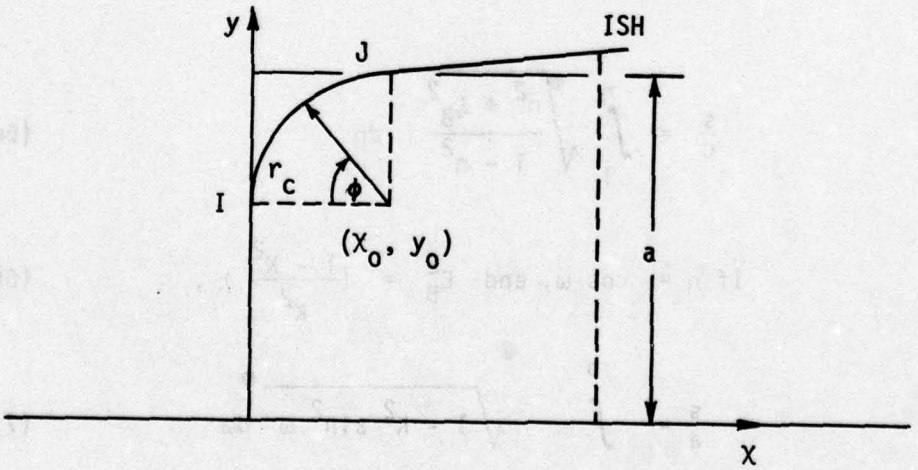

Sketch 3. Flat Face - Round Shoulder Coordinates

The intersection point between the shoulder and flat face is

$$\chi_I = 0 \tag{10a}$$

$$y_I = s_I = a - r_c \tag{10b}$$

The intersection of the corner and aft body is

$$\chi_J = r_c - \frac{r_c \tan \theta_c}{\sqrt{1 + \tan^2 \theta_c}} \tag{11a}$$

$$y_J = y_I + \frac{r_c}{\sqrt{1 + \tan^2 \theta_c}} \tag{11b}$$

$$\theta_J = \frac{\pi}{2} - \theta_c \tag{11c}$$

$$s_J = s_I + r_c \phi_J \tag{11d}$$

The shoulder point (*ISH*) is

$$\chi_{ISH} = r_c \tag{12a}$$

$$y_{ISH} = y_J + (r_c - \chi_J) \tan \theta_c \tag{12b}$$

$$s_{ISH} = s_J + [(y_{ISH} - y_J)/\sin \theta_c] \tag{12c}$$

The center of the shoulder (χ_o, y_o) is

$$\chi_o = r_c \tag{13a}$$

$$y_o = a - r_c \tag{13b}$$

The equations for χ, θ, and s on the flat face are

$$\chi = 0 \tag{14a}$$

$$\theta = \pi/2 \tag{14b}$$

$$s = y \tag{14c}$$

On the corner

$$x = r_c - \sqrt{r_c^2 - (y - y_o)^2} \tag{15a}$$

$$\phi = \sin^{-1} \left\{ \frac{y - y_o}{r_c} \right\} \tag{15b}$$

$$\theta = \frac{\pi}{2} - \phi \tag{15c}$$

$$s = s_I + r_c \phi \tag{15d}$$

On the flank, $y > y_J$, the equations are the same as those for the ellipsoid, i.e., Equations 9a, 9b, and 9c.

3. SPHERICAL ARC - ROUND CORNER

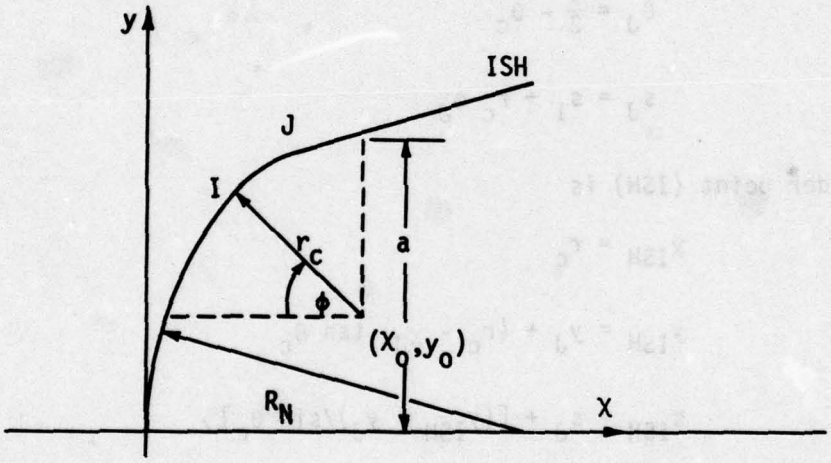

Sketch 4. Spherical Arc - Round Corner Coordinates

Center of corner (x_o, y_o)

$$y_o = a - r_c \tag{16a}$$

$$x_o = R_N - \sqrt{R_N^2 - y_o^2} \tag{16b}$$

Intersection of arcs (x_I, y_I)

$$\phi_I = \sin^{-1} \left\{ \frac{y_o}{R_N - r_c} \right\} \tag{17a}$$

$$y_I = R_N \frac{y_o}{(R_N - r_c)} \tag{17b}$$

$$x_I = R_N (1 - \cos \phi_I) \tag{17c}$$

$$s_I = R_N \phi_I \tag{17d}$$

Intersection of corner with flank (x_J, y_J)

$$\phi_J = \frac{\pi}{2} - \theta_c \tag{18a}$$

$$y_J = y_o + r_c \cos \theta_c \tag{18b}$$

$$x_J = x_o - r_c \sin \theta_c \tag{18c}$$

$$s_J = s_I + r_c (\phi_J - \phi_I) \tag{18d}$$

Shoulder location (x_{ISH}, y_{ISH})

$$x_{ISH} = x_o \tag{19a}$$

$$y_{ISH} = y_I + (x_o - x_J) \tan \theta_c \tag{19b}$$

$$s_{ISH} = s_J + \frac{(y_{ISH} - y_J)}{\sin \theta_c} \tag{19c}$$

The equations for the dependent variables over the different regions are:
On spherical arc $(y \leq y_I)$

$$\phi = \sin^{-1} (y/R_N) \tag{20a}$$

$$x = R_N - \sqrt{R_N^2 - y^2} \tag{20b}$$

$$\theta = \frac{\pi}{2} - \phi \tag{20c}$$

$$s = R_N \phi \tag{20d}$$

On corner ($y_I < y \leq y_J$)

$$\phi = \sin^{-1} \left(\frac{y - y_o}{r_c}\right) \tag{21a}$$

$$x = x_o - r_c \cos \phi \tag{21b}$$

$$\theta = \frac{\pi}{2} - \phi \tag{21c}$$

$$s = s_I + r_c (\phi - \phi_I) \tag{21d}$$

On shoulder ($y_I < y \leq y_{ISH}$)

$$x = x_J + \frac{(y - y_J)}{\tan \theta_c} \tag{22a}$$

$$s = s_J + \frac{(y - y_J)}{\sin \theta_c} \tag{22b}$$

$$\theta = \theta_c \tag{22c}$$

It is also noteworthy to consider the case of the sharp corner. For θ_J greater than 10°, a discontinuity will exist at the corner.

$$y_J = y_{ISH} = a \tag{23a}$$

$$x_J = x_{ISH} = R_N - \sqrt{R_N^2 - a^2} \tag{23b}$$

For θ_J less than 10°, the nose will flare smoothly into the aft body.

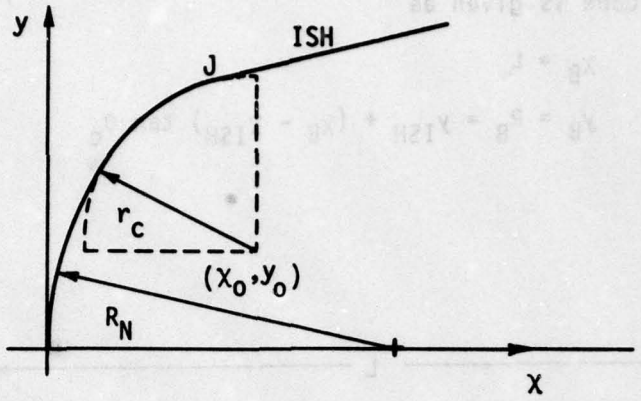

Sketch 5. Spherical Arc - Round Shoulder, $\theta_J < 10°$

$$\phi_J = \frac{\pi}{2} - \theta_c \tag{24a}$$

$$y_J = R_N \sin \phi_J \tag{24b}$$

$$x_J = R_N (1 - \cos \phi_J) \tag{24c}$$

$$s_J = R_N \phi_J \tag{24d}$$

and,

$$x_{ISH} = R_N \tag{25a}$$

$$y_{ISH} = y_J + (x_{ISH} - x_J) \tan \theta_c \tag{25b}$$

$$s_{ISH} = s_J + [(y_{ISH} - y_J)/\sin \theta_c] \tag{25c}$$

4. AFT BODY OF CONE

For the aft body, s is the independent variable and

$$x = x_{ISH} + (s - s_{ISH}) \cos \theta_c \tag{26a}$$

$$y = y_{ISH} + (s - s_{ISH}) \sin \theta_c \tag{26b}$$

$$\theta = \theta_c \tag{26c}$$

The end of the cone is given as

$$x_B = L \tag{27a}$$

$$y_B = R_B = y_{ISH} + (x_B - x_{ISH}) \tan \theta_c \tag{27b}$$

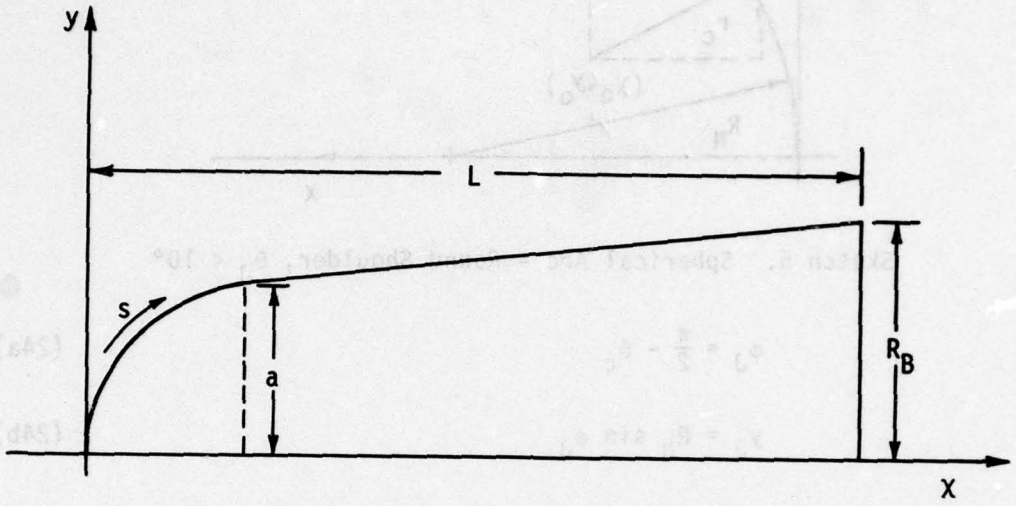

Sketch 6. Aft Body Coordinate System

SECTION III

INVISCID CALCULATIONS

In this section the methods used to calculate the inviscid local flow properties are presented. Empirical methods available in the literature were used. Real gas effects were accounted for by determining an effective specific heat ratio.

1. FREESTREAM CONDITIONS

The freestream conditions at a given altitude were determined from equations given by Dommasch, Sherby and Connolly (Reference 7). The sea level values are as follows:

$$P_{SL} = 2116.217 \text{ lbf/ft}^2$$

$$\rho_{SL} = 0.002377 \text{ slugs/ft}^2$$

$$T_{SL} = 518.688 \text{ °R}$$

$$a_{SL} = 1116.444 \text{ ft/sec}$$

$$g_{SL} = 32.174 \text{ ft/sec}^2$$

$$R_{er} = 20{,}855{,}531.0 \text{ ft}$$

The distance above the earth's surface is the geometric altitude, h_G. The distance from the earth's center is the absolute altitude, h_a. The geopotential altitude, h_g is given by

$$h_g = h_G; \; h_G \leq 60{,}000 \text{ ft} \tag{28a}$$

$$h_g = \frac{R_{er} h_G}{h_a}; \; h_G > 60{,}000 \text{ ft} \tag{28b}$$

In the geopotential layers where g is essentially constant, the pressure, density and temperature are given as follows:

Isothermal region (T = constant):

$$\delta = \delta_1 \, e^{\varepsilon} \tag{29a}$$

$$\sigma = \sigma_1 \, e^{\varepsilon} \tag{29b}$$

Gradient Region (dT/dh_G is constant):

$$T = T_1 + a_d (h_g - h_b) = T_i + a_d h_g \tag{30a}$$

$$\delta = \delta_1 (T/T_1)^{-1/a_d r} \tag{30b}$$

$$\sigma = \sigma_1 (T/T_1)^{-[1/a_d R + 1]} \tag{30c}$$

where

$$\varepsilon = \frac{h_b - h_g}{RT} \quad , \quad a_d = \frac{dT}{dh_G}$$

and h_b, δ_1, σ_1, T_1 and y are given in Table 1.

$$1/a_d R$$

The freestream stagnation properties are calculated from the relationships using the static values of P_∞, T_∞, and ρ_∞ and the freestream values of M_∞ and γ.

$$T_{o_\infty} = T_\infty \left[1 + \frac{\gamma-1}{2} M_\infty^2 \right] , (°R) \tag{31a}$$

$$P_{o_\infty} = P_\infty \left[1 + \frac{\gamma-1}{2} M_\infty^2 \right]^{\frac{\gamma}{\gamma-1}} , \frac{lbf}{ft^2} \tag{31b}$$

$$\rho_{o_\infty} = \rho_\infty \left[1 + \frac{\gamma-1}{2} M_\infty^2 \right]^{\frac{1}{\gamma-1}} , \frac{slugs}{ft^3} \tag{31c}$$

The stagnation enthalpy was determined as follows

$$h_{o_\infty} = C_p T_\infty + \frac{V_\infty^2}{2Jg_c} \tag{32}$$

2. SHOCK DENSITY RATIO

If h_{o_∞} is less than 864.0 BTU/lbm, the isentropic gas equations can be used to determine the shock density ratio. For h_{o_∞} greater than 864.0 BTU/lbm, real-gas effects must be considered and an iteration procedure is required.

TABLE 1

ATMOSPHERIC CONSTANTS

Thermal Layer	h_G, ft	h_b, ft	$a_d = \frac{dT}{dh_G}$, °F/1000 ft	T_1, °R	δ_1	σ_1	1/aR
1	0	0	-3.566160	518.688	1	1	-5.256113706
2	36,152	36,089	0	389.988	0.223359	0.297069	0
3	82,345	82,021	+1.645920	254.988	0.0245606	0.0326657	+11.3882463
4	155,348	154,199	0	508.788	0.00118866	0.00121179	0
5	175,346	173,885	-2.46888	938.088	5.75968×10^{-4}	5.86784×10^{-4}	-7.5921646
6	262,448	259,186	0	289.188	9.96102×10^{-6}	1.73274×10^{-5}	0
7	299,516	295,276	+2.19456	-349.812	1.03055×10^{-6}	1.792653×10^{-6}	+8.5411853

Ideal Gas ($h_{0_\infty} \leq 864$ BTU/lbm)

$$\frac{\rho_2}{\rho_\infty} = \frac{\gamma + 1}{(\gamma-1) + \frac{2}{M_1^2}} \tag{33a}$$

$$\frac{T_2}{T_1} = \frac{[2\gamma M_\infty^2 - (\gamma-1)][(\gamma-1)M_\infty^2 + 2]}{(\gamma+1)^2 M_\infty^2} \tag{33b}$$

$$\frac{P_2}{P_\infty} = 1 + \frac{2\gamma}{\gamma+1}(M_\infty^2 - 1) \tag{33c}$$

$$M_2 = \frac{(\gamma-1) M_\infty^2 + 2}{2\gamma M_\infty^2 - (\gamma-1)} \tag{33d}$$

Real Gas ($h_{0_\infty} > 864$ BTU/lbm)

The computational procedure for the real-gas case is as follows:

(1) Guess ρ_2 (isentropic relationships)

ITERATION

(2) $u_2 = \rho_\infty u_\infty / \rho_2$

(3) $P_2 = P_\infty + \rho_\infty u_\infty^2 - \rho_2 u_2^2$

(4) $h_2 = h_\infty + \frac{1}{2}(u_\infty^2 - u_2^2)$

(5) $\rho_2 = \rho_2 (h_2, P_2)$; Bade (Reference 19)

The iteration is continued until the percent change in the density is less than 1×10^{-6}.

Knowing the density, pressure and enthalpy behind the shock, a temperature is calculated from the perfect gas equations. If the temperature is less than 2500°R, the following equations were used.

$$\gamma - 1 = \frac{0.4}{1 + 0.4\left(\frac{5500}{T}\right)^2 \frac{e^{(5500/T)}}{[e^{5500/T}-1]^2}} \tag{34a}$$

$$M_2 = \frac{u_2}{\sqrt{\gamma R T_2}} \tag{34b}$$

If T_2 is greater than 2500°R, then the temperature behind the shock is calculated from Hansen (Reference 8). Because of its complexity, this method is not presented here.

The stagnation conditions behind the shock are calculated as follows:

$$M_2 = u_2/\sqrt{\gamma R T_2}$$

ITERATION

$$P_{o_2} = P_2 + \frac{1}{2}\rho_2 u_2^2 \left[1 + \frac{M_2^2}{4}\right] \tag{34c}$$

$$\rho_{o_2} = P_{o_2}(H_o, P_{o_2}); \text{ Bade (Reference 19)} \tag{34d}$$

$$T_{o_2} = T_{o_2}(P_{o_2}, h_{o_2}, \rho_{o_2}); \text{ Hansen (Reference 8)} \tag{34e}$$

$$\gamma_{eff} = \ell n\,(P_2/P_{o_2})/\ell n\,(\rho_2/\rho_{o_2}) \tag{34f}$$

$$M_2 = u_2/\sqrt{\gamma_{eff} R T_2} \tag{34g}$$

The iteration is continued until the change in M_2 is less than 0.001.

3. SHOCK WAVE CALCULATIONS

The shock stand-off distance, radius of curvature and profile were calculated from Krasnov (Reference 9), and James and Terry (Reference 10). The shock stand-off distance and radius of curvature for the three different nose shapes are as follows.

a. Sphere

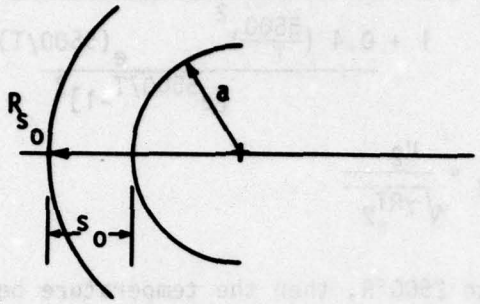

Sketch 7. Hemisphere Shock Stand-off

Shock stand-off:

$$\frac{S_o}{a} = \overline{S}_h = 0.78125\ \overline{\rho}\ ;\quad \overline{\rho} = \frac{\rho_\infty}{\rho_2} \tag{35a}$$

Radius of curvature:

$$\frac{R_{s_o}}{a} = \overline{R}_{s_h} = 0.78125 \left\{ 1.0 + \sqrt{\frac{8}{3}\,\overline{\rho}} \right\} \tag{35b}$$

b. Flat-Face Sharp Corner

$$\frac{S_o}{a} = \overline{S}_f = 1.03 \sqrt{\frac{\overline{\rho}}{1-\overline{\rho}}} \tag{36a}$$

$$\overline{R}_{s_f} = \left(\frac{R_{s_o}}{a} \right)_f = \frac{1.03 \left[1 + \sqrt{\frac{8}{3}\,\overline{\rho}} \right]}{[1.0 + 0.78125\overline{\rho}] \sqrt{\overline{\rho}\ (1.0 - \overline{\rho})}} \tag{36b}$$

c. Flat Face-Round Corner

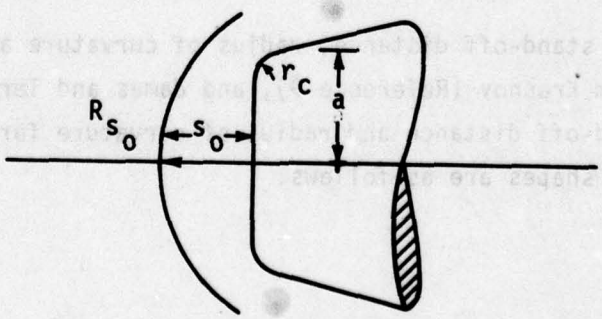

Sketch 8. Flat Face - Round Shoulder Shock Stand-off

$$\bar{S}_o = \frac{S}{a} = \bar{S}_f - [\bar{S}_f - \bar{S}_h] \frac{r_c}{a} \tag{37a}$$

$$\bar{R}_{s_o} = \frac{\bar{R}_{s_f} \bar{R}_{s_h}}{\bar{R}_{s_h} + \left[\bar{R}_{s_f} - \bar{R}_{s_h}\right] \frac{r_c}{a}} \tag{37b}$$

d. Oblate Ellipsoid

The shock stand-off distance for the oblate ellipsoid was adjusted to fit the trends given by Felderman et al (Reference 11).

$$\bar{S}_e = \bar{S}_f \, e^{[e_1(b/a) + e_2(b/a)^2]} \tag{38}$$

The constants e_1, and e_2 are calculated from $\bar{S}_h$ and $\bar{S}_{0.5}$. A simultaneous solution gives

$$e_1 = 4\ell n \{0.025 + 1.1814\ \bar{\rho}\} - \ell n\ (\bar{S}_h) - 3\ \ell n\ (\bar{S}_f) \tag{39a}$$

$$e_2 = 2\ \ell n\ (\bar{S}_h) + 2\ \ell n\ (\bar{\rho}_f) - 4\ \ell n\ (0.025 + 1.1814\ \bar{\rho}) \tag{39b}$$

$$\bar{S}_{0.5} = 0.025 + 1.1814\ \bar{\rho} \tag{39c}$$

The radius of curvature of the shock can be determined as follows

$$\tilde{S}_o = \frac{S_o}{R_{s_o}} = \frac{\bar{S}_o}{\bar{R}_{s_o}} \tag{40a}$$

therefore,

$$\frac{R_{s_o}}{a} = \frac{\bar{S}_o}{\tilde{S}_o} \tag{40b}$$

then,

$$\tilde{S}_h = \frac{\bar{\rho}}{1 + \sqrt{\frac{8}{3}\ \bar{\rho}}}, \text{ and } \tilde{S}_f = \frac{(1.0 + 0.78125\ \bar{\rho})}{\bar{S}_h} \tag{40c}$$

Assume that $\tilde{S}_o$ varies linearly with (b/a), then

$$\tilde{S}_e = \tilde{S}_f - (\tilde{S}_f - \tilde{S}_h)(b/a) \tag{41a}$$

and

$$\overline{R}_{s_o} = \overline{S}_e/\tilde{S}_e = \overline{S}_e/[\tilde{S}_f - (\tilde{S}_f - \tilde{S}_h)(b/a)] \tag{41b}$$

where $\overline{S}_e$ is given by Equation 38.

e. Spherical Arc - Sharp Corner

The shock stand-off distance and shock radius of curvature for the spherical arc nose shapes are given in this section. Results presented in Krasnov (Reference 9) show that the shock stand-off varies linearly with (Δ/a).

$$\left(\frac{S_o}{a}\right)_{SA} = \left(\frac{S_o}{a}\right)_f - \frac{20}{9}\left[\left(\frac{S_o}{a}\right)_f - 2\left(\frac{S_o}{a}\right)_h\right]\frac{\Delta}{a} \tag{42}$$

where

$$\frac{\Delta}{a} = \frac{R_N}{a}\left[1.0 - \sqrt{1.0 - \left(\frac{a}{R_N}\right)^2}\right] \tag{43}$$

Equation 42 is assumed to be valid for when the sonic point is on the corner, i.e. $0 \leq (\Delta/a) \leq \overline{\Delta}_*$. The sonic point is assumed to be at the corner for $\theta_j \geq 45°$. Therefore $\overline{\Delta}_* = 0.41421$, for a nose body radius (a) of one inch.

For (Δ/a) larger than $\overline{\Delta}_*$, the shock stand-off distance must decrease monotonically to the value for the hemisphere. This is accomplished by matching a second order polynomial to a straight line through $(s/a)_h$.

$$(S_o/a)_h = C_o + C_1\,\tilde{\Delta} + C_2\,\tilde{\Delta}^2 \tag{44a}$$

where

$$C_o = \overline{S}_f - \frac{20}{9}\left[\overline{S}_f - 2\,\overline{S}_h\right]\overline{\Delta}_c \tag{44b}$$

$$C_1 = -\frac{20}{9}\left[\bar{S}_f - 2\bar{S}_h\right] \tag{44c}$$

and,

$$\tilde{\Delta} = \bar{\Delta} - \bar{\Delta}_* \tag{44d}$$

The match point of the polynomial and straight line is assumed to be

$$\tilde{\Delta}_{MP} = \frac{-2.0\,(C_o - \bar{S}_h)}{C_1} \tag{45}$$

therefore

$$C_2 = \frac{C_o + C_1\tilde{\Delta}_h - \bar{S}_h}{\left[\tilde{\Delta}_{MP} - 2\tilde{\Delta}_h\right]\tilde{\Delta}_{MP}} \tag{46a}$$

where

$$\tilde{\Delta}_h = 1.0 - \bar{\Delta}_* \tag{46b}$$

also,

$$m_{SA} = \frac{C_1 + 2.0\left[C_o + C_1\tilde{\Delta}_h - \bar{S}_h\right]}{\left[\tilde{\Delta}_{MP} - 2\tilde{\Delta}_h\right]} \tag{46c}$$

and,

$$b = \bar{S}_h - m_{SA}\,\tilde{\Delta}_h \tag{46d}$$

The polynomial expression is used from $\bar{\Delta}_* \le \bar{\Delta} \le (\bar{\Delta}_* + \tilde{\Delta}_{MP})$. The linear expression $\bar{S} = b + m\tilde{\Delta}$ is used from $(\bar{\Delta}_* + \tilde{\Delta}_{MP})$ to 1.0.

An expression for the shock radius of curvature is given by Krosnov as

$$\left(\frac{R_{s_o}}{a}\right) = \frac{\bar{R}_{s_f} B_s}{B_s + \frac{20}{9}\left[R_{s_f} - B_s\right]\bar{\Delta}} \tag{47}$$

where B_s is given as the value of $\bar{R}_{s_o}$ at $\bar{\Delta} = 0.45$ and is approximately equal to 1.8 to 2 times $\bar{R}_{sh_o}$. For this investigation B_s is taken as $\frac{20}{9}$ $\bar{R}_{sh_o}$, which is somewhat larger, and the above equation is used over the full range of $\bar{\Delta}$.

f. Spherical Arc - Round Corner

For the rounded corner spherical arc, the shock stand-off and shock radius of curvature are assumed to vary as follows:

$$\bar{S}_o = \bar{S}_{SA} - [\bar{S}_{SA} - \bar{S}_h](r_c/a) \tag{48a}$$

$$\bar{R}_s = \frac{(\bar{R}_s)_{SA}\,(\bar{R}_s)_h}{(\bar{R}_s)_h - [(\bar{R}_s)_h - (\bar{R}_s)_{SA}](r_c/a)} \tag{48b}$$

g. Shock Wave Profile

The shock wave profile can be determined from James and Terry (Reference 10).

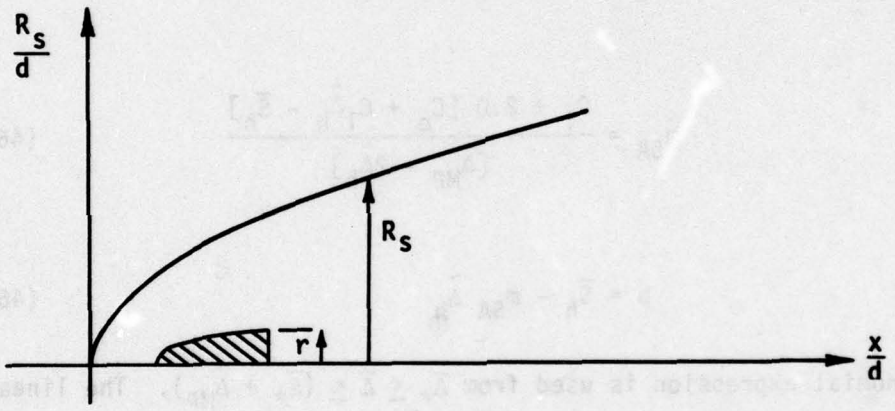

Sketch 9. Shock Wave Profile

$$\frac{R_s}{a} = k_s \left\{ \left(\frac{x}{d}\right)^{\frac{1}{n}} + a_s \left(\frac{x}{a}\right) \right\}^n \tag{49}$$

where

$$k_s = \frac{1}{\sqrt{M_\infty^2 - 1}} + 0.057\, C_{D_N}^{1.35}\, M_\infty^{-0.0687} \tag{50a}$$

$$a_s = 0.56 \left\{ C_{D_N}^{0.75} (M_\infty^2 - 1) \right\}^{0.2741 + 1.15 \left[C_{D_N}^{0.75} (M_\infty^2 - 1) \right]^{-0.07}} \tag{50b}$$

$$n = \frac{0.646 \exp\left(-0.237\, C_{D_N}^{0.75}\right)}{\left[C_{D_N}^{0.5} M_\infty^2 \right]^{0.034}} \tag{50c}$$

where C_{D_N} is the drag coefficient for the different nose shapes.

4. PRESSURE DISTRIBUTION

The inviscid pressure distribution over the reentry body was considered in three parts: the nose, after body and base. There are many methods available for calculating the pressure distribution over the nose of a hypersonic vehicle. These methods however are complicated and time consuming. For the purposes of this investigation, a simplified method was desired that would give relatively accurate results between shapes as well as short computer times.

a. Oblate Ellipsoid

Vinokur's method (References 12, 13, and 14) is used for calculating the pressure distribution over the oblate ellipsoids. This method gives good results for the flat faced shape but is somewhat less accurate for the hemisphere. The method is developed in detail in Reference 15, and is summarized here for completeness.

The nondimensional pressure (P/P_{o_2}) is given by

$$\frac{P}{P_{o_2}} = 1.0 - \frac{k\left(A_v - B_v \eta^2\right)^2}{(2.0 - k)} \left[\frac{1.0 - \eta^2}{\xi_B^2 + \eta^2} \right] \tag{51}$$

where $k = P_\infty/P_2$, and ξ_B, η are elliptic coordinates given by

$$\xi_B = b/c \tag{52a}$$

$$\eta = \frac{(b/a)\tan\theta}{\sqrt{1 + (b/a)^2 \tan^2\theta}} \tag{52b}$$

The terms A & B are constants given by

$$A_v = \frac{2B_2}{(\xi_B^2 + 1)} + \frac{16\,B_4}{(\xi_B^2 + 1)(5\xi_B^2 + 1)} + \frac{K^2\,\xi_B^3(\xi_B^2 + 1)}{(5\xi_B^2 + 1)} \tag{53a}$$

and

$$B_v = \frac{80\,B_4}{(\xi_B^2 + 1)(5\xi_B^2 + 1)} - \frac{K^2\,\xi_B^2(\xi_B^2 + 1)}{(5\xi_B^2 + 1)} \tag{53b}$$

where

$$B_2 = \frac{0.5 - 0.4\,\bar{\lambda}\,K_v - C_2\,K_v^2}{C_1} \tag{54a}$$

$$B_4 = \frac{-0.10\,\bar{\lambda}\,K_v - C_6\,K_v^2}{C_4} \tag{54b}$$

$$K_v = \left[\frac{1-k}{k}\right]\left[\frac{S_o/R_{s_o}}{S_o/a}\right]\frac{1}{\sqrt{\xi_B^2 + 1}} \tag{54c}$$

$$\bar{\lambda} = -(P_1K_v + P_2) \pm \sqrt{(P_1K_v+P_2)^2 - (P_3K_v+0.20)} \tag{54d}$$

(use sign which gives $\bar{\lambda} < \bar{\xi}_s$)

$$\bar{\xi}_s = \xi_b + \left(\frac{S_o}{a}\right)\sqrt{\xi_B^2 + 1} \tag{55a}$$

$$P_1 = \frac{(\bar{\xi}_s^2 + 1)}{10} \tag{55b}$$

$$P_2 = - P_1 \frac{C_8}{C_4} - 0.40\ \bar{\xi}_s \tag{55c}$$

$$P_3 = 2(\bar{\xi}_s^2 + 1)\left[C_7 - C_6 \frac{C_8}{C_4}\right] \tag{55d}$$

The constants C_1, C_2, C_4, C_6, C_7, and C_8 are

$$C_1 = \frac{\bar{\xi}_s}{\bar{\xi}_s^2 + 1} + \tan^{-1}\bar{\xi}_s - d_1 \tag{56a}$$

$$C_2 = \frac{\bar{\xi}_s^2 - \xi_B^2}{10} \tag{56b}$$

$$C_4 = 15\ \bar{\xi}_s - \frac{2\ \bar{\xi}_s}{(\bar{\xi}_s^2 + 1)} + (5\bar{\xi}_s^2 + 1)\left[3\tan^{-1}\bar{\xi}_s - d_2\right] \tag{56c}$$

$$C_6 = \frac{\xi_B^2 - \bar{\xi}_s^2}{10(1 + 5\xi_B^2)} \tag{56d}$$

$$C_7 = \frac{-\bar{\xi}_s}{5(5\ \xi_B^2 + 1)} \tag{56e}$$

$$C_8 = 10\ \bar{\xi}_s\ (3\tan^{-1}\bar{\xi}_s - d_2) + \left\{\frac{16 + 50\ \bar{\xi}_s^2 + 30\bar{\xi}_s^4}{(\bar{\xi}_s^2 + 1)}\right\} \tag{56f}$$

The constants d_1 and d_2 are

$$d_1 = \frac{\xi_B}{(\xi_B^2 + 1)} + \tan^{-1} \xi_B \tag{57a}$$

$$d_2 = \frac{15\xi_B}{(5\xi_B^2 + 1)} - \frac{2\xi_B}{(1 + \xi_B^2)(5\xi_B^2 + 1)} + 3 \tan^{-1} \xi_B \tag{57b}$$

b. Flat Face - Round Shoulder

The pressure distribution on the flat face - round shoulder nose was determined by assuming a velocity distribution from the stagnation point to the sonic point. A modified Newtonian type equation was used from the sonic point to the Prandtl-Meyer match point.

The velocity distribution was assumed to be linear from the stagnation point to S_L, i.e., $u = (du/ds)_{SP}s$, where

$$s_L = 0.70\ (1.0 - r_c/a)s_f^* \tag{58}$$

Beyond s_L, the velocity is assumed to vary parabolically to the sonic point S*, i.e.,

$$u = u_L + \left(\frac{du}{ds}\right)_{SP} (s-s_L) + C_3\ (s-s_L)^2 \tag{59}$$

where

$$C_3 = \frac{u^* - u_L - (du/ds)_{SP}\ (s^* - s_L)}{(s^* - s_L)^2} \tag{60}$$

The corresponding pressure is determined from the isentropic relationships.

A modified Newtonian type equation is used aft of the sonic point on the rounded corner.

$$\frac{P}{P_{o_2}} = \left(\frac{P^*}{P_{o_2}}\right) - K_p \sin^2 (\theta^* - \theta) - J_p(\theta^* - \theta) \tag{61}$$

where,

$$J_P = \frac{d\bar{p}^*}{d\theta} \quad ; \text{ slope at the sonic point} \tag{62a}$$

$$K_P = \frac{(\bar{P}^* - \bar{P}_\infty) - J_P\theta^*}{\sin^2 \theta^*} \; ; \; \bar{P}^* = \frac{P^*}{P_{o_2}} \tag{62b}$$

The value for J_P was determined as follows:

$$\frac{d\bar{p}^*}{d\theta} = \frac{d\bar{p}^*}{du^*} \frac{du^*}{ds^*} \frac{ds^*}{d\theta} \tag{63}$$

where

$$\frac{ds^*}{d\theta} = -r_c \tag{64a}$$

$$\frac{du^*}{ds^*} = \left(\frac{du}{ds}\right)_{SP} + 2\, C_3\, (s^* - s_L) \tag{64b}$$

$d\bar{p}^*/du^*$ is determined from the isentropic relationships and M = 1.0,

$$\frac{d\bar{p}^*}{du^*} = \frac{d\bar{p}^*}{dM^2} \frac{dM^2}{du^*} = -\frac{\gamma u^*}{a_{02}^2} \left(\frac{\gamma+1}{2}\right)^{\frac{-1}{\gamma-1}} \tag{65}$$

therefore

$$\frac{d\bar{p}^*}{d\theta} = \frac{\gamma u^*\, r_c}{a_{02}^2 (s^*-s_L)} \left(\frac{\gamma+1}{2}\right)^{\frac{-1}{\gamma-1}} \left[2(u^*-u_L) - \left(\frac{du}{ds}\right)_{SP} (s^*-s_L)\right] \tag{66}$$

This method is used from the sonic point to the Prandtl-Meyer match point.

c. Spherical Arc

The spherical arc pressure distribution was calculated in a manner similar to that for the flat face because a modified Newtonian

pressure distribution fails to give the proper stagnation point velocity gradient and sonic point location. The linear velocity region is given by

$$s_L = \left[1.0 - \frac{r_c}{a}\right]\left[1.0 - \frac{a}{R_N}\right]\left[0.70 - \frac{0.10}{0.70}\left(\frac{a}{R_N}\right)\right] s_f^* \qquad (67)$$

This gives the same results for the flat face and hemisphere as the equation for the flat - round case. The term

$$\left[0.70 - \frac{0.10}{0.70}\left(\frac{a}{R_N}\right)\right]$$

is required in order to prevent an inflection point occurring in the velocity distribution. The equations for the velocity distribution in the subsonic region are the same as for the flat face - round shoulder case. The method for calculating the pressure distribution aft of the sonic point is also the same. This method gives results which are identical to the flat face - round corner nose for both the hemisphere and the flat face nose shapes.

The methods for calculating the pressure distributions over the various nose shapes are used up to the point where a match is obtained with the Prandtl-Meyer pressure. This occurs when the pressure and pressure gradients are equal to those given by the Prandtl-Meyer theory.

$$\left(P/P_{o_2}\right)_{PM} = \left(P/P_{o_2}\right) \qquad (68a)$$

$$\left(\frac{d\ P/P_{o_2}}{d\theta}\right)_{PM} = \frac{d}{d\theta}\left(\frac{P}{P_{o_2}}\right) \qquad (68b)$$

where

$$\frac{d}{d\theta}\left(\frac{P}{P_{o_2}}\right)_{PM} = \frac{\left[\left(\frac{2\gamma}{\gamma-1.0}\right)\left[\left(\frac{P}{P_{o_2}}\right)^{1/\gamma} - \left(P/P_{o_2}\right)\right]\right]}{\left\{\frac{2}{(\gamma-1.0)}\left[\frac{P}{P_{o_2}}\right]^{\frac{1-\gamma}{\gamma}} - \frac{20}{\gamma-1.0} - 1.0\right\}} \qquad (69)$$

For the oblate ellipsoid nose

$$\frac{d\bar{p}}{d\theta} = \frac{d\bar{p}}{d\eta}\,\frac{d\eta}{d\theta} \tag{70a}$$

where

$$\frac{d\theta}{d\eta} = \frac{\xi_B}{\xi_B^2 + \eta^2}\sqrt{\frac{1 + \xi_B^2}{1 - \eta^2}} \tag{70b}$$

$$\frac{d\bar{p}}{d\theta} = \frac{2\eta k}{(2 - k)}\,\frac{(A_v - B_v\eta^2)}{(\xi_B^2 + \eta^2)^2}\sqrt{\frac{1 - \eta^2}{1 + \xi_B^2}}$$

$$X\,\{2B_v(1 - \eta^2)(\xi_B^2 + \eta^2) + (A_v - B_v\eta^2)(\xi_B^2 + 1)\} \tag{70c}$$

For the flat face - round shoulder and spherical arc noses, the pressure gradient is

$$\frac{d\bar{p}}{d\theta} = K_p \sin 2\,(\theta^* - \theta) + J_p \tag{71}$$

The match point location is determined using an iteration procedure. Knowing the match point angle, θ_{mp}, and Mach number, M_{mp}, the Prandtl-Meyer relationship is used to determine the Mach number distribution over the nose. The isentropic relationship is then used to calculate the associated pressure.

The effects of mass addition on the inviscid pressure over the nose was neglected (Reference 16).

d. Aft Body Pressure Distribution

The pressure distribution on the aft body can be determined from a method given by Krasnov (Reference 9) which takes into account the nose bluntness effects on the aft body distribution. This method is good for for $\chi \geq \chi_{ISH} + 2a$. For the region between χ_J and $\chi_{SH} + 2a$, an exponential relationship was used to insure that no inflection points occurred between X_J and $X_{su} + 2a$.

$$\bar{P} - \bar{P}_{MIN} = A_o \exp\left[A_1 (\chi'/a) + A_2 (\chi/a)^2\right] \tag{72}$$

where χ' is measured from χ_J, and $\bar{P}_{MIN}$ is from Krasnov.

The constants A_o, A_1, and A_2 are determined from the following boundary conditions:

1. $\chi = \alpha_J$, $X' = 0$: $\bar{P}_J$ & $(d\bar{p}/d\theta)_J$ are known from nose calculations.

2. $\chi' = \chi'_{MIN}$: $(d\bar{p}/d\chi) = 0$

These boundary conditions give

$$A_o = \bar{P}_J - \bar{P}_{MIN} \tag{73a}$$

$$A_1 = \frac{(d\bar{p}/d\chi)_J \, a}{A_o} \tag{73b}$$

$$A_2 = \frac{-A_1}{2.0\bar{\chi}'_{MIN}} \quad ; \; \bar{\alpha}'_{MIN} = \frac{\alpha'_{MIN}}{\alpha} \tag{73c}$$

In order to determine A_1, $(d\bar{p}/d\chi)_J$ must be known. This can be determined from $(d\bar{p}/d\theta)_J$

$$\left(\frac{d\bar{p}}{d\chi}\right)_J = \left(\frac{d\bar{p}}{d\theta}\right)_J \left(\frac{d\theta}{d\chi}\right)_J \tag{74}$$

Therefore, $(d\theta/d\chi)_J$ must be known for each of the different types of nose shapes.

1d. Oblate Ellipsoid

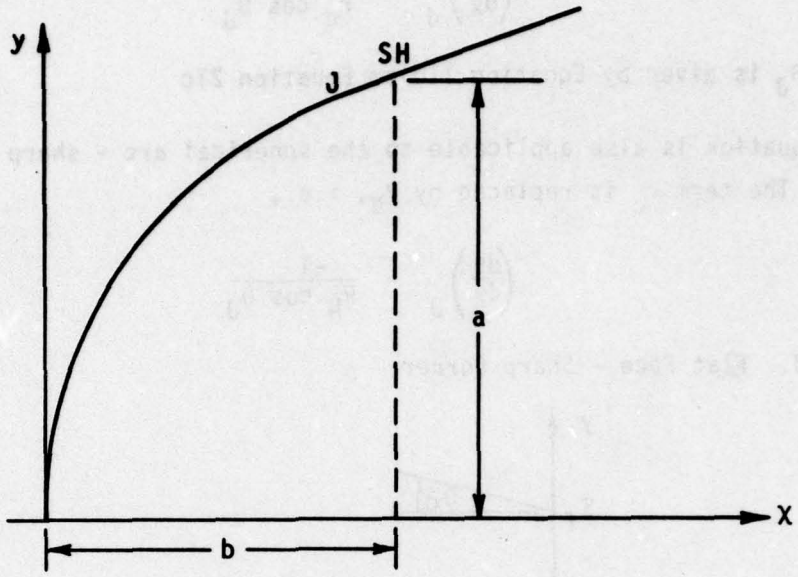

Sketch 10. Oblate Ellipsoid Nose Notation

$$\left(\frac{d\theta}{d\chi}\right)_J = -\left[\frac{\sin\theta\cos\theta}{(b-\chi)\left(\frac{y^2}{c^2}\frac{1}{1+\xi_B^2}\right)}\right]_J \tag{75}$$

where χ_J, y_J, and θ_J are given by equations 2 and 8b, respectively

2d. Rounded Corners (Flat Face or Spherical Arc)

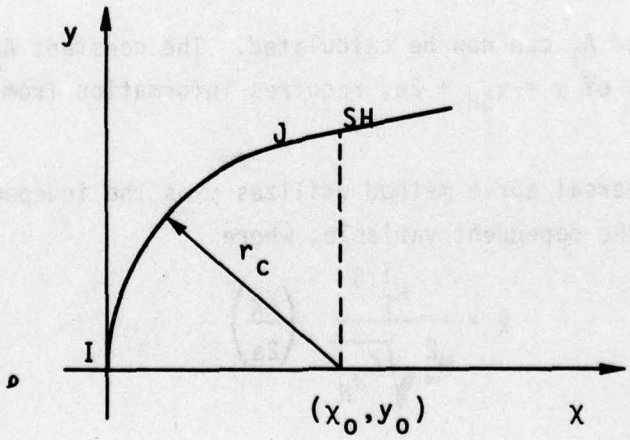

Sketch 11. Round Corner Notation

$$\left(\frac{d\theta}{d\chi}\right)_J = \frac{-1}{r_c \cos \theta_J} \tag{76}$$

where θ_J is given by Equation 11c or Equation 21c

This equation is also applicable to the spherical arc - sharp corner case. The term r_c is replaced by R_N, i.e.,

$$\left(\frac{d\theta}{d\chi}\right)_J = \frac{-1}{R_N \cos \theta_J} \tag{77}$$

3d. Flat Face - Sharp Corner

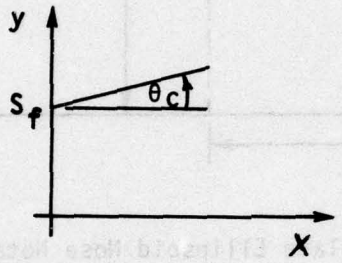

Sketch 12. Flat Face - Sharp Shoulder Notation

on the flank $\chi = (S - S_f) \cos \theta_c$, and $d\chi/d\theta = 0$.

For this case use $(d\bar{p}/ds)_J$

$$\left(\frac{d\bar{p}}{d\chi}\right)_J = \left(\frac{d\bar{p}}{ds}\right)_J \left(\frac{ds}{dx}\right)_J ; \quad \frac{ds}{dx} = \frac{1}{\cos \theta_c} \tag{78}$$

The constants A_o and A_1 can now be calculated. The constant A_2, as well as the pressure aft of $\chi = \chi_{SH} + 2a$, requires information from the universal curve.

Krasnov's universal curve method utilizes $\tilde{\chi}$ as the independent variable and $\tilde{P}$ as the dependent variable, where

$$\tilde{\chi} = \frac{K_1^{1.5}}{M_\infty^2 \sqrt{C_{D_N}}} \left(\frac{\chi_K}{2a}\right) \tag{79a}$$

$$\tilde{P} = \frac{K_1^{0.2} C_p}{(\tan \theta_c)^{1.8}} \tag{79b}$$

and

$$K_1 = M_\infty \tan \theta_c \tag{79c}$$

$$C_p = (P - P_\infty)/\tfrac{1}{2} \rho_\infty u_\infty^2 \tag{79d}$$

where χ_k is measured from χ_{SH}.

This curve (Reference 9, Page 606) was digitized as follows:

$\tilde{X}$	$\tilde{P}$
.05	1.475
.10	1.240
.12	1.200
.14	1.200
.15	1.230
.20	1.350
.25	1.480
.30	1.550
.35	1.600
.40	1.650
.50	1.680
.60	1.740
.70	1.770
.80	1.780
.90	1.790
1.00	1.800

The minimum was estimated to occur at $\tilde{X}_{MIN} = 0.13$, with $\tilde{P}_{MIN} = 1.20$.

Using Equation 79a,

$$\chi_{K_{MIN}} = 2a\, \tilde{\chi}_{MIN} \frac{M_\infty^2}{K_1^{1.5}} \sqrt{C_{D_N}} \tag{80}$$

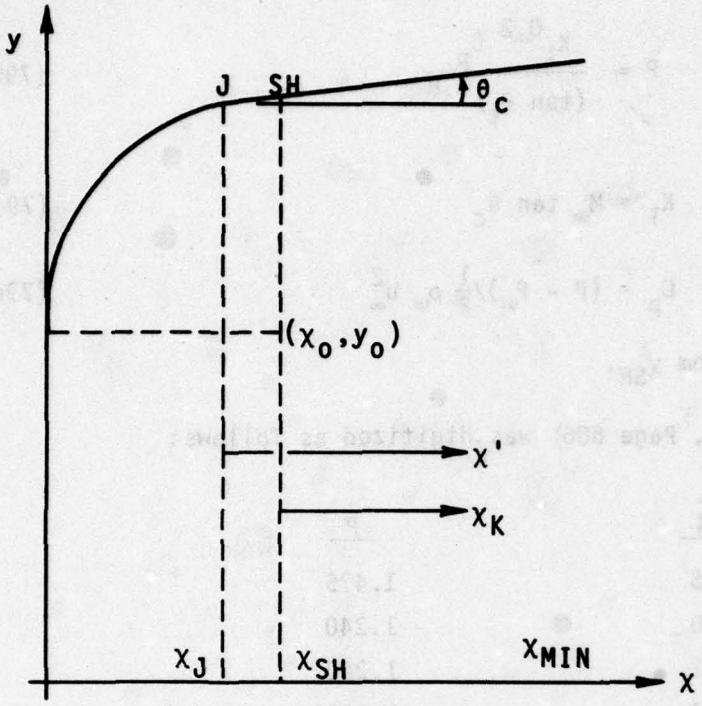

Sketch 13. Shoulder Region Notation

$$x_{MIN} = x_{SH} + x_{k_{MIN}} \tag{81a}$$

$$x'_{MIN} = (x_{SH} - x_J) + x_{k_{MIN}} \tag{81b}$$

$$\bar{x}'_{MIN} = x'_{MIN}/a \tag{81c}$$

$$\text{and } A_2 = -A_1\, a/(2.0\, x'_{MIN}) \tag{81d}$$

The method used in computer program is to use the expotential relationship, Equation 72, between x_J and x_{MIN}, and then for $x > x_{MIN}$, the universal curve is used. Linear interpolation is used for values of $\tilde{x}$ that fall between the tabulated values. The pressure distribution obtained in this manner was considered to be adequate for the purposes of this investigation, i.e., no corrections were made for curved shock effects or boundary layer effects on the aft body.

Knowing the universal pressure distribution over the body, the value for velocity, temperature, and density can be obtained from the isentropic relationships:

$$\left[1 + \frac{\gamma-1}{2} M^2\right] = \left(P/P_{o_2}\right)^{-\frac{\gamma-1}{\gamma}} \tag{82a}$$

$$\frac{u^2}{a_{02}^2} = M^2 \left(1 + \frac{\gamma-1}{2} M^2\right)^{-1} \tag{82b}$$

$$\frac{T}{T_{o_2}} = \left[1 + \frac{\gamma-1}{2} M^2\right]^{-1} \tag{82c}$$

$$\frac{\rho}{\rho_{o_2}} = \left[1 + \frac{\gamma-1}{2} M^2\right]^{\frac{-1}{\gamma-1}} \tag{82d}$$

where γ is obtained from Equation 34f, and $a_{o_2} = \sqrt{\gamma R T_{o_2}}$.

The enthalpy is obtained from

$$h = H_o - \frac{u_e^2}{2 g_c J} \tag{82e}$$

5. SONIC POINT LOCATION AND STAGNATION POINT VELOCITY GRADIENT

In order to calculate the pressure distribution on the flat face - round shoulder noses and the spherical arc noses, the stagnation point velocity gradient and sonic point location must be known.

a. Flat Face - Round Shoulder

The sonic point location for the flat face - round shoulder nose shapes was assumed to vary linearly with respect to (r_c/a) as follows:

$$s^* = s^*_{flat} - [s^*_{flat} - s^*_{hemi}] (r_c/a) \tag{83}$$

b. Spherical Arc - Sharp Shoulder

For the spherical arc - sharp corner nose shape, the sonic point was assumed to be fixed at the corner for $\theta_{corner} \geq 45°$. For $\theta_{corner} < 45°$, the sonic point was assumed to vary as follows:

$$s^* = s^*_{hemi} + b_1 (Z - Z_{hemi}) + b_2 (Z - Z_{hemi})^2 \tag{84a}$$

where

$$Z = (a/R_N)^{-1} \quad ; \quad Z_{hemi} = 1.0 \tag{84b}$$

$$b_1 = a \sin^{-1} \left\{ \sqrt{\frac{1 - \bar{P}^*}{1 - \bar{P}_\infty}} \right\} \tag{84c}$$

$$b_2 = \frac{S^*_{\theta=45°} - S^*_{hemi} - b_1 (Z_{\theta=45°} - Z_{hemi})}{(Z_{\theta=45°} - Z_{hemi})^2} \tag{84d}$$

The above expression for s* was based on a modified Newtonian type variation for s*, i.e.,

$$s^*_{\substack{Mod \\ Newtonian}} = \left[a \sin^{-1} \left\{ \sqrt{\frac{1 - \bar{P}^*}{1 - \bar{P}_\infty}} \right\} \right] \left(\frac{a}{R_N} \right)^{-1} \tag{85}$$

c. Spherical Arc - Round Shoulder

For the rounded shoulder case, the sonic point was assumed to vary with respect to (r_c/a).

$$s^* = s^*_{SC} - (s^*_{SC} - s^*_{hemi})(r_c/a) \tag{86}$$

where s^*_{SC} is the value for the sharp corner.

The stagnation point velocity gradients were determined from results given by Boison and Curtiss (Reference 7). The stagnation point velocity gradient for the different noses was assumed to vary with respect to (X^*/y^*) as follows:

$$J_s \left(\frac{du}{ds}\right)_{SP} = \left[J_s \left(\frac{du}{ds}\right)_{SP}\right]_{hemi} \left\{ \left[J_s \left(\frac{du}{ds}\right)_{SP}\right]_{hemi} - \left[J_s \left(\frac{du}{ds}\right)_{SP}\right]_{flat} \right\}$$

$$\left\{ \frac{\left(\frac{X^*}{y^*}\right)_B - \left(\frac{X^*}{y^*}\right)_{hemi}}{\left(\frac{X^*}{y^*}\right)_{flat} - \left(\frac{X^*}{y^*}\right)_{hemi}} \right\} \qquad (87a)$$

where

$$\frac{J_s}{y^*} = \frac{1.0}{\sqrt{\frac{2P_{o_2}}{\rho_{o_2}} (1 - \overline{P}_\infty)}} \qquad (87b)$$

and

$$\left[J_s \left(\frac{du}{ds}\right)_{SP}\right]_{flat} \quad \text{and} \quad \left[J_s \left(\frac{du}{ds}\right)_{SP}\right]_{hemi}$$

are determined from Vinokur's method.

SECTION IV

VISCOUS CALCULATIONS

This section describes the methods used to obtain quantitative information concerning the viscous flow effects. The viscous calculations are more difficult than the inviscid calculations. The two calculations are of course coupled and under certain circumstances this interaction cannot be ignored. In addition there are the added complications of mass addition, transition and real gas effects. A solution to the entire viscous problem is not required here and use is made of the many approximations that exist in the literature.

1. VISCOSITY

The viscosity is determined from an empirical correlation to Sutherland's formula developed by Hansen and Heims (Reference 18).

$$\mu = \begin{cases} \mu_s & T < 6000°R \\ K_s \mu_s & T \geq 6000°R \end{cases} \tag{88a}$$

where Sutherland's law provides

$$\mu_s = 0.227 \times 10^{-7} \frac{T^{3/2}}{T + 198.6} \left(\frac{\text{slugs}}{\text{ft-sec}}\right) \tag{88b}$$

where T is in °R

and,

$$K_s = \frac{1.0 + \frac{0.023\ T}{1800.0} \left\{1.0 + \tanh\left[\frac{\frac{T}{1800}\ (1.0 - 0.125A_\mu) - 6.5}{1.5 + 0.125A_\mu}\right]\right\}}{1.0 + \exp\left(\frac{\frac{T}{1800} - 14.5 - 1.5\ A_\mu}{0.9 + 0.10\ A_\mu}\right)} \tag{88c}$$

where

$$A_\mu = \log_{10}(P_a)\ ;\quad P_a \text{ is in atm} \tag{88d}$$

and $K_s \geq 0.04$

2. DENSITY

The density is determined from a method given by Bade (Reference 19).

$$\frac{\rho}{\rho_1} = \left[\frac{P}{P_1}\right] \left[\frac{h}{h_1}\right]^{-X_\rho} \tag{89a}$$

where

$$X_\rho = 0.70 + 0.04 \log_{10} (P/P_1) \tag{89b}$$

$$h_1 = 31.9\ RT_o = 1080\ \text{BTU/lbm} \tag{89c}$$

$$P_1 = 1\ \text{atm} = 2116.22\ \text{lbf/ft}^2 \tag{89d}$$

$$\rho_1 = 0.124\ \rho_{SL} = 0.00949\ \text{lbm/ft}^3 \tag{89e}$$

range $31.9 \leq \frac{h}{RT_o} \leq 480$; $0.1\ \text{atm} \leq P \leq 100\ \text{atm}$

The above equation is valid to within 5% at pressures considerably greater than 100 atm over the enthalpy range indicated.

For the range $3.8 \leq h/RT_o \leq 31.9$, $0.1 \leq P(\text{atm}) \leq 100$, $X_o = 0.94$

(In this region ρ/P is nearly independent of pressure.)

3. LOCAL HEAT TRANSFER AND SKIN FRICTION

There are many methods available for estimating the heat transfer and skin friction on a flat plate in a uniform flow. These methods can also be used for a sharp cone through the use of a simple correction factor, if it is assumed that the local body radius is much greater than the boundary-layer thickness. The essential characteristic of these methods is a zero pressure gradient. However, most shapes of interest have a nonzero pressure gradient at the boundary layer edge, which complicates the solution. For regions where the pressure gradient is not too strong, the advantages of the simpler zero pressure gradient methods outweigh the increase in accuracy of the nonzero pressure gradient methods.

For this investigation, where only a relative accuracy is necessary, Eckert's (Reference 20) "reference enthalpy" method was used to predict the heat transfer and skin friction downstream of the stagnation point. This method is not only easy to apply but is applicable to both laminar and turbulent flows. Introducing properties evaluated at the reference enthalpy causes the effect of compressibility on the friction factor to vanish, thus validating the use of the incompressible solutions for both laminar and turbulent flows.

As determined empirically by Eckert

$$h^* = 0.5\,(h_w + h_e) + 0.22\,(h_r - h_e) \tag{90}$$

where h_w is the wall enthalpy, h_e is the boundary layer edge enthalpy, and h_r is the recovery enthalpy, given by

$$h_r = h_e + r_f \left(\frac{u_e^2}{2\,J\,g_c}\right), \quad \frac{BTU}{lbm} \tag{91}$$

where the recovery factor, r_f, is $Pr^{1/2}$ for laminar flow and $Pr^{1/3}$ for turbulent flow.

The wall temperature of the nose was assumed to be constant (2000°R), thus h_w can be determined from

$$h_w = C_p\,T_w \tag{92}$$

where C_p was assumed a constant.

The heat transfer at the stagnation point was calculated from the Fay-Riddell equation

$$(\dot{q})_{\substack{no\\blowing}} = 0.763\,Pr^{-2/3} \left(\frac{\rho_w\,\mu_w}{\rho_{o_2}\,\mu_{o_2}}\right) \sqrt{\rho_{o_2}\,\mu_{o_2}\,u_w} \sqrt{\frac{1}{u_\infty}\left(\frac{du}{ds}\right)_{SP}}\,(h_o - h_w) \tag{93}$$

where Pr was assumed to have a value of 0.71. A slight improvement can be obtained by using expression given by Fox & Libby (Reference 21),

$$Pr = 0.525\,T^{0.07}$$

For laminar heating downstream of the stagnation point, Lees (Reference 52) equations were used in conjunction with the reference enthalpy method.

$$\left(\frac{\dot{q}^*}{\dot{q}_o}\right)_{\text{no blowing}} = \frac{F^*(s)}{F^*(o)} \tag{94}$$

where

$$F^*(s) = \frac{\frac{\sqrt{2}}{2}\left[\frac{\rho^*\mu^*}{\rho_{o_2}\mu_{o_2}}\right]\left[\frac{u_e}{u_\infty}\right] y}{\left[\int_o^s \frac{\rho^*\mu^*}{\rho_{o_2}\mu_{o_2}} \frac{u_e}{u_\infty} y^2\, ds\right]^{1/2}} \tag{95a}$$

and

$$F^*(o) = \sqrt{\frac{2}{u_\infty}\frac{\rho^*\mu^*}{\rho_{o_2}\mu_{o_2}}\left(\frac{du}{ds}\right)_{SP}} \tag{95b}$$

The laminar skin friction was calculated from

$$C_{f_o} = 0.664\sqrt{zC^*/Re_s} \tag{96a}$$

where

$$C^* = \rho^*\mu^*/\rho_e\mu_e \tag{96b}$$

and Re_s, is the edge Reynolds number

$$Re_s = \frac{\rho_e u_e s}{\mu_e} \tag{96c}$$

The turbulent skin friction was calculated from an expression given by Langanelli et al., (Reference 23).

$$\frac{C_{f_o}}{2} = 0.0296\, M_f\, \varepsilon_T\, Re^{1/5} \tag{97a}$$

where

$$\varepsilon_T = \left(\frac{\rho^*}{\rho_e}\right)^{4/5} \left(\frac{\mu^*}{\mu_e}\right)^{1/5} \tag{97b}$$

and

$$M_f = 1.176 \tag{97c}$$

The turbulent Stanton number can be calculated using Reynolds Analogy

$$St_o = \frac{C_{f_o}}{2}\, Pr_T^{-2/3} \tag{98}$$

The turbulent Prandtl number (Pr_T) was assumed to have a value of one.

The turbulent heat transfer was calculated as follows:

$$(\dot{q})_{\substack{\text{no}\\ \text{blowing}}} = \rho_e u_e (h_r - h_w)\, St_o \tag{99}$$

The above expression for heat transfer and skin friction were corrected for diffusion as follows:

$$DC_{Lam} = \left[1 + (Le^{\beta} - 1)\, \frac{h_D}{(h_r - h_w)}\right] \tag{100a}$$

$$DC_{Turb} = \left[1 + 0.4\, \frac{h_D}{(h_r - h_w)}\right] \tag{100b}$$

Where Le is the Lewis number, and was assumed to be constant (Le = 1.45). A value of 0.53 was assumed for β corresponding to equilibrium flow.

The enthalpy of dissociation h_D is given by Krasnov (Reference 9).

$$h_D = h_r - C_p T \left(\frac{T}{T_o}\right)^{\phi} \tag{101a}$$

$$T_o = 273°K$$

$$\phi = 0.1; \; T > 1000°K \tag{101b}$$

The above equations were corrected for mass addition by utilizing expression given in Timmer, Arne, et al. (Reference 24).

For laminar flow:

$$\frac{C_f}{C_{f_o}} = \frac{St}{St_o} = 1.0 - 0.68\, W^{0.4}B + 0.08\, W^{0.4}B^2 \tag{102a}$$

While for turbulent flow:

$$\frac{C_f}{C_{f_o}} = \frac{St}{St_o} = \frac{W^{0.8}B}{\left[1 + \frac{W^{0.8}B}{4}\right]^4 - 1} \tag{102b}$$

The specific heat ratio, W, was assumed to have a constant value of 1.86. This is for water vapor to air and was given in Gold (Reference 25).

The blowing parameter, B, is defined as

$$B = \dot{m}/\rho_e u_e St_o \tag{103}$$

The mass addition is assumed to be the minimum, i.e.,

$$\dot{m} = \dot{q}/\Delta H_c \tag{104}$$

where ΔH_c is the total enthalpy rise of the coolant. For the case of water, a constant value of 1150 BTU/lbm was assumed.

The blowing parameter can then be expressed as follows:

$$B_{Lam} = \frac{(a_1 + \bar{H}) - \sqrt{a_1^2 - 4a_2 + 2a_1\bar{H} + \bar{H}^2}}{2a_2} \quad (105a)$$

$$B_{Turb} = \frac{4}{a_3}\left\{\left(\frac{a_3 + \bar{H}}{\bar{H}}\right)^{1/4} - 1\right\} \quad (105b)$$

where

$$a_1 = 0.68\ W^{0.4} \quad (105c)$$

$$a_2 = 0.08\ W^{0.4} \quad (105d)$$

$$a_3 = W^{0.8} \quad (105e)$$

$$\bar{H} = \Delta H_c/(h_r - h_w) \quad (105f)$$

The coolant distribution is then given by

$$\dot{m} = \frac{B}{(h_r - h_w)}\ \dot{q}_o \quad (106)$$

where $\dot{q}_o$ is the no blowing heat transfer to the surface of the nose tip. The cooling extended only to the end of the nose region. On the aft cone, no cooling calculations were performed.

4. TRANSITION FROM LAMINAR TO TURBULENT

Any number of methods for estimating the transition point appear in the literature. For simplicity sake, transition was assumed to occur when the Reynolds number, based on the blowing momentum thickness, equaled three hundred, i.e.,

$$Re_{\theta_T} = 300 \quad (107)$$

This value is in line with that given by Van Driest (Reference 26) as well as Cresci, MacKenzie, and Libby (Reference 27).

The Reynolds number based on the blowing momentum thickness if given by

$$Re_\theta = \frac{\rho_e u_e \delta^{**}}{\mu_e} \tag{108}$$

The value for the laminar momentum thickness with blowing was determined from Timmer, Arne, et al. (Reference 24) as

$$\frac{\delta^{**}}{\delta_o^{**}} = \frac{C_f}{C_{f_o}} + B \tag{109}$$

where

$$\delta_o^{**} = 0.4696\ S \sqrt{\frac{2\ C^*}{3\ Re_s}} \tag{110}$$

5. TRANSVERSE CURVATURE AND VISCOUS INTERACTION

The effect of transverse curvature is to decrease the boundary-layer thickness and correspondingly increase the skin friction and heat transfer. This effect is small for turbulent boundary layers and hence is omitted in these calculations. The effect of boundary layer thickness on the inviscid pressure distribution is also neglected.

SECTION V

TRAJECTORY CALCULATIONS

1. GOVERNING EQUATIONS

The reentry trajectory of a non-lifting vehicle can be calculated for a non-rotating earth from the following equations:

$$1/2\ \rho_\infty\ V_\infty^2\ C_D\ A_B = -m\ V_\infty + mg \sin\gamma \tag{111a}$$

$$m\ V_\infty\ (\dot{\Phi} + \dot{\gamma}) = mg \cos\gamma \tag{111b}$$

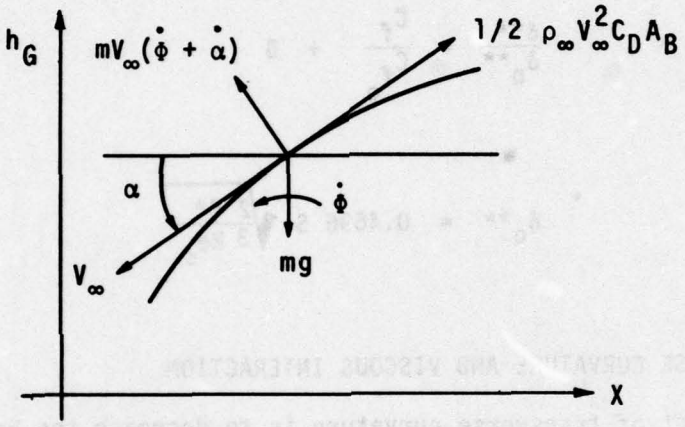

Sketch 14. Trajectory

The centrifugal force term, $m\ V_\infty\ \dot{\Phi}$, can be expressed as

$$\dot{\Phi} = \frac{V_\infty \cos\gamma}{(R_{er} + h_G)} \tag{112}$$

where R_{er} is the radius of the earth ($2.09 \times 10^{+7}$ ft), and h_G is the altitude of the vehicle. The reentry equations may be written as

$$\frac{dh_G}{dt} = \dot{h}_G = -V_\infty \sin\gamma \tag{113a}$$

$$\frac{dX}{dt} = \dot{X} = -V_\infty \cos\gamma \tag{113b}$$

then,

$$\frac{dV_\infty}{dt} = g \sin \gamma - 1/2\, \rho_\infty \frac{C_D\, A_B\, V_\infty^2}{m} \tag{113c}$$

and

$$\frac{d\gamma}{dt} = \left[\frac{g}{V_\infty} - \frac{V_\infty}{(R_{er} + h_G)} \right] \cos \gamma \tag{113d}$$

The independent variable is the time, t, and the unknowns are V_∞, γ, h_G, and X. The Runge-Kutta method is used to solve for the above unknowns for a given time step.

A time step of two seconds was found to be satisfactory for altitudes above 60,000 feet. Below this altitude a one second time step was used and when impact was imminent, the time step was calculated from

$$\Delta t = 0.9\, h_G / V_\infty \sin \gamma \tag{114}$$

Impact was considered to occur when the altitude was less than 10 feet. The Runge-Kutta method requires initial starting conditions which for this investigation were assumed to be:

Altitude	=	300,000 ft
Velocity	=	25,000 ft/sec
Angle	=	20 deg
Weight	=	800 lb

2. PRESSURE DRAG

The drag of the vehicle must be calculated at each point in time in order to solve for the unknowns at the next time point. The total drag of the vehicle is the sum of the pressure, skin friction and base drag. The skin friction and pressure drag are determined by integrating the local values over the surface area of the vehicle. The pressure drag was calculated from

$$D_P = \int_A (P_e - P_\infty) \sin \theta \, dA \tag{115a}$$

3. SKIN FRICTION DRAG

The skin friction was determined from

$$D_{sf} = \int_A \tau \cos \theta \, dA \tag{115b}$$

For a conical body the element area can be expressed as

$$dA = 2\pi y \, ds = 2\pi y \left(\frac{ds}{dy}\right) dy \tag{116}$$

where the term (ds/dy) for the different nose shapes is given as follows:

Oblate ellipsoid:

$$\frac{ds}{dy} = \frac{c}{a}\sqrt{\frac{(a/c)^2 - (y/a)^2}{1 - (y/a)^2}} \tag{117}$$

Flat nose - round shoulder:

a) Flat region: $ds/dy = 1.0$ (118a)

b) Corner region: $$\frac{ds}{dy} = \frac{r_c}{\sqrt{r_c^2 - (y-y_o)^2}} \tag{118b}$$

Spherical arc - round shoulder:

a) Large arc: $$\frac{ds}{dy} = \frac{R_N}{\sqrt{R_N^2 - y^2}} \tag{119a}$$

b) Corner region: $$\frac{ds}{dy} = \frac{r_c}{\sqrt{r_c^2 - (y-y_o)^2}} \tag{119b}$$

Aft cone: $$\frac{ds}{dy} = \frac{1}{\sin \theta_c} \tag{120}$$

The integration can be carried out using any numerical integration method. The Romberg method, which is explained in detail by Carnahan, et al., (Reference 29) was used for this investigation.

4. BASE DRAG

The base drag of a conical vehicle was determined from an empirical equation given by Hoerner (Reference 28).

$$C_{D_B} = \frac{\gamma_\infty}{2M_\infty^2} \tag{121}$$

5. TOTAL COOLANT

Knowing the altitude and velocity for a given time the coolant was calculated using the method discussed in the preceding sections. The total coolant required over the trajectory is of course the summation of the coolant used at each time step. The trapezoidal integration method was used to obtain this value because the time intervals over the trajectory were not equal and the number of points on each trajectory varied. The expression used to determine the total coolant was

$$\text{Total coolant}_{\,i} = \text{Total coolant}_{\,(i-1)} + 1/2\,[\dot{M}_i + \dot{M}_{i-1}][t_i - t_{i-1}] \tag{122}$$

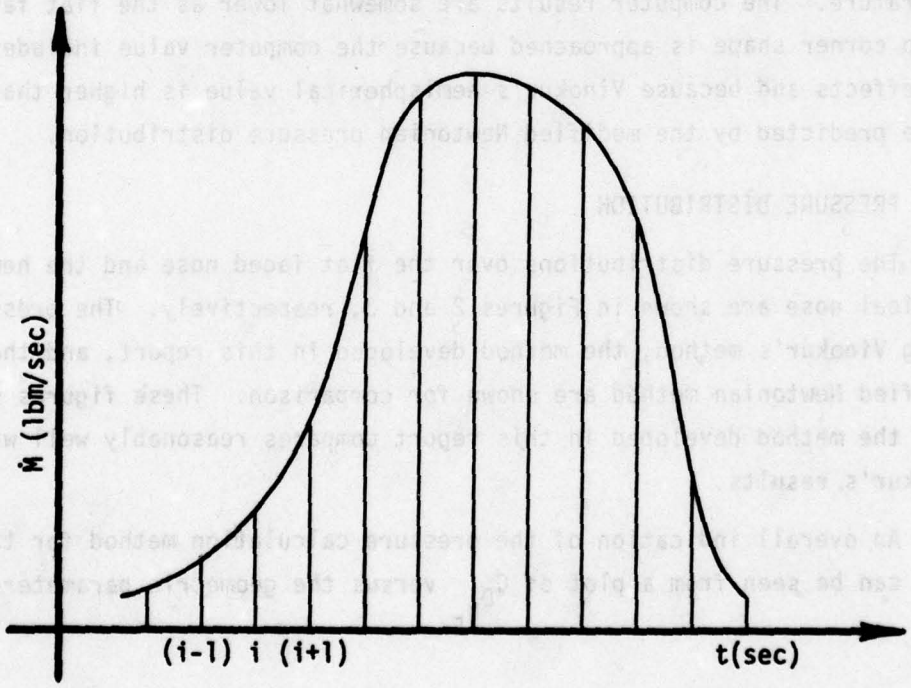

Sketch 15. Total Coolant

SECTION VI

COMPUTER PROGRAM VALIDATION

The system of equations presented in the previous sections were programmed for use on the CDC 6600 computer, and this section discusses the validation of that program. Values generated by the computer program are compared either with theory or with data available in the literature.

1. STAGNATION POINT VELOCITY GRADIENT

A comparison of the stagnation point velocity gradients with the literature gives an indication of the validity of not only the method for determining the velocity gradient but also the method for calculating the sonic point location. The stagnation point velocity gradients for the three different nose shapes are plotted in Figure 1. The open symbols are from the computer program. The closed symbols represent data from the literature (References 17 and 34). As can be seen the trends predicted by the computer program agrees qualitatively with results in the literature. The computer results are somewhat lower as the flat face - sharp corner shape is approached because the computer value includes real gas effects and because Vinokur's hemispherical value is higher than the value predicted by the modified Newtonian pressure distribution.

2. PRESSURE DISTRIBUTION

The pressure distributions over the flat faced nose and the hemispherical nose are shown in Figures 2 and 3, respectively. The pressures using Vinokur's method, the method developed in this report, and the modified Newtonian method are shown for comparison. These figures show that the method developed in this report compares reasonably well with Vinokur's results.

An overall indication of the pressure calculation method for the nose can be seen from a plot of $C_{D_{N_E}}$ versus the geometric parameters

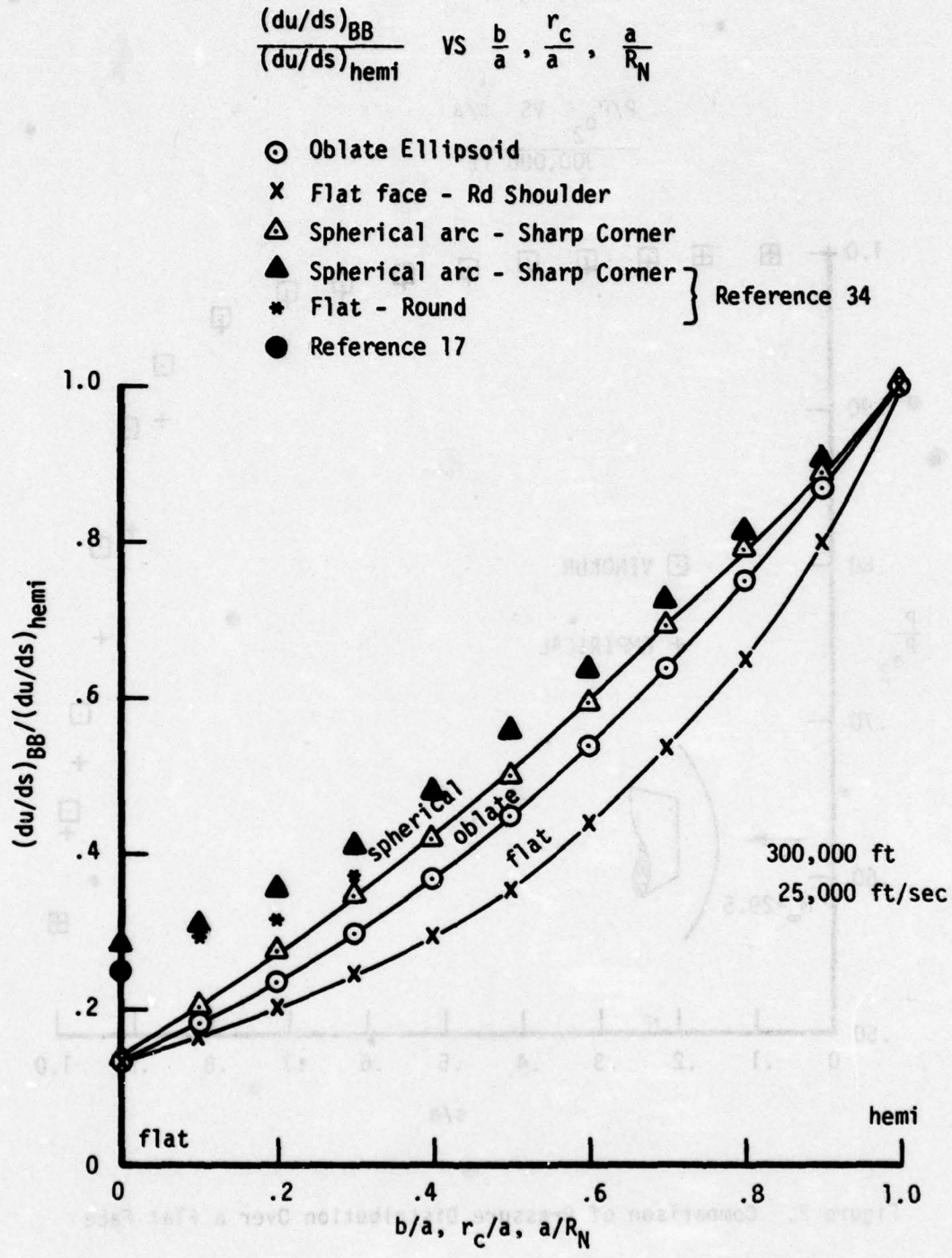

Figure 1. Stagnation Point Velocity Gradients

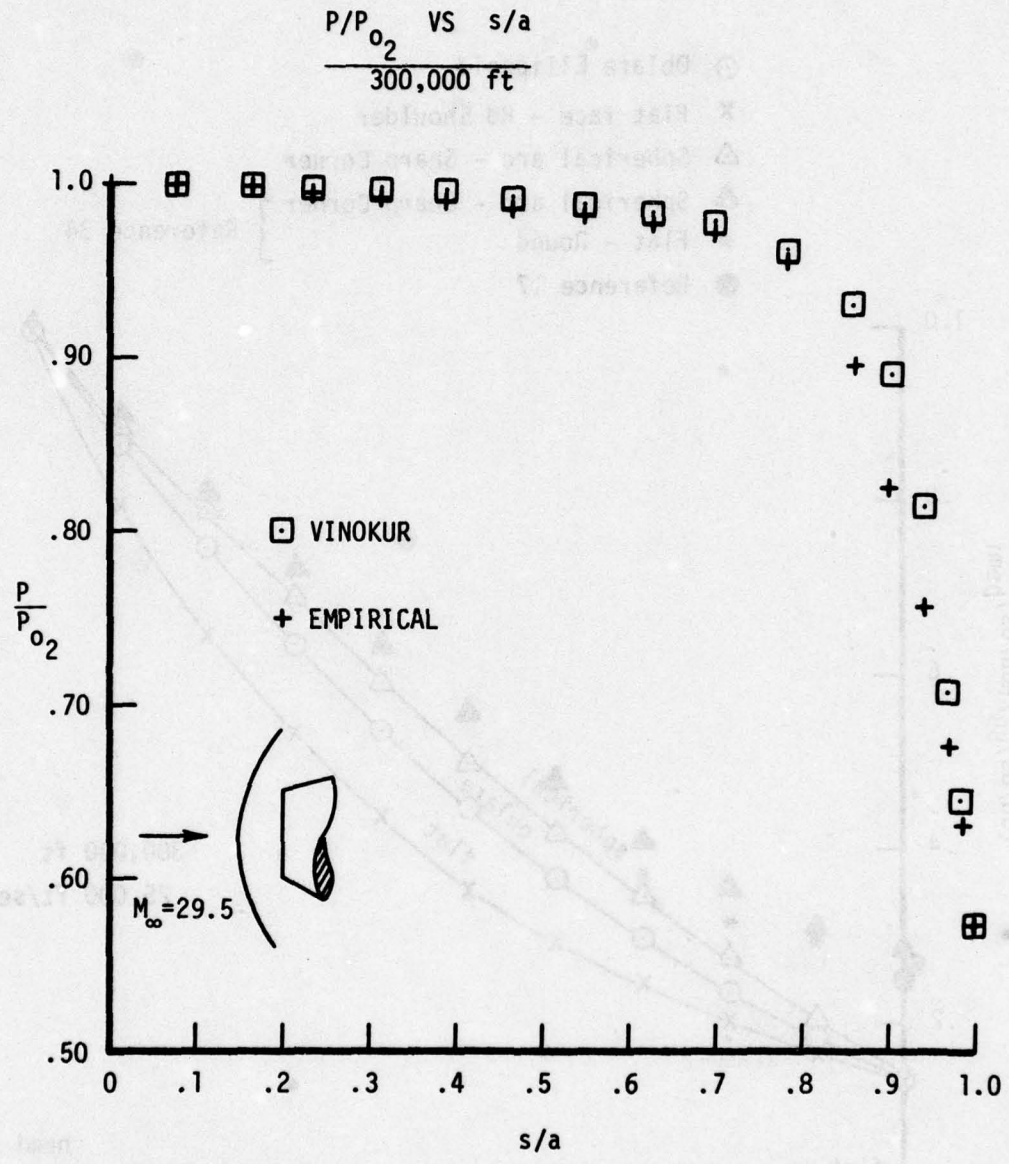

Figure 2. Comparison of Pressure Distribution Over a Flat Face

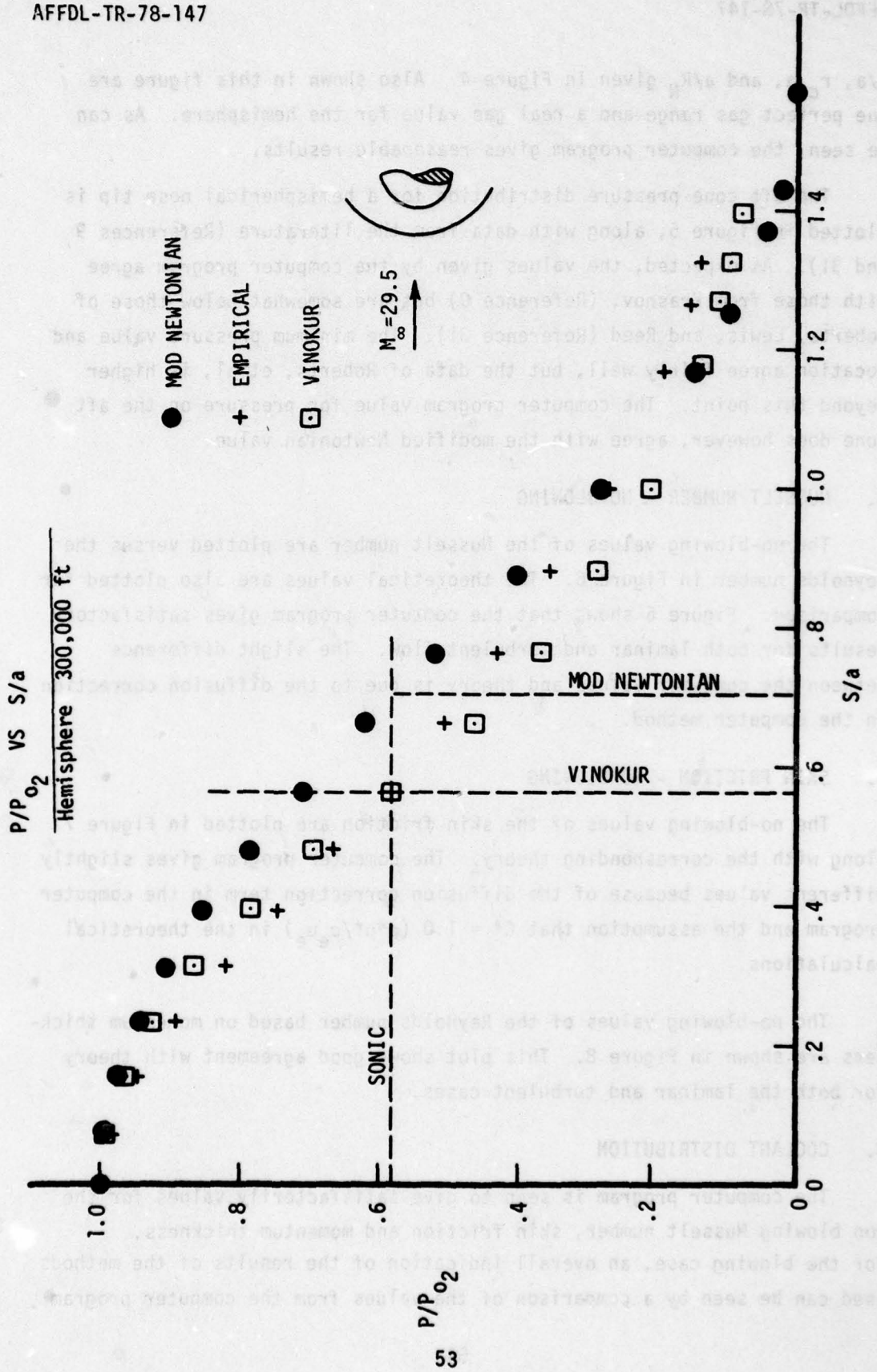

Figure 3. Comparison of Pressure Distribution Over a Hemisphere

b/a, r_c/a, and a/R_N given in Figure 4. Also shown in this figure are the perfect gas range and a real gas value for the hemisphere. As can be seen, the computer program gives reasonable results.

The aft cone pressure distribution for a hemispherical nose tip is plotted in Figure 5, along with data from the literature (References 9 and 31). As expected, the values given by the computer program agree with those from Krasnov, (Reference 9) but are somewhat below those of Roberts, Lewis, and Reed (Reference 31). The minimum pressure value and location agree fairly well, but the data of Roberts, et al, is higher beyond this point. The computer program value for pressure on the aft cone does however, agree with the modified Newtonian value.

3. NUSSELT NUMBER - NO BLOWING

The no-blowing values of the Nusselt number are plotted versus the Reynolds number in Figure 6. The theoretical values are also plotted for comparison. Figure 6 shows that the computer program gives satisfactory results for both laminar and turbulent flow. The slight difference between the computer values and theory is due to the diffusion correction in the computer method.

4. SKIN FRICTION - NO BLOWING

The no-blowing values of the skin friction are plotted in Figure 7 along with the corresponding theory. The computer program gives slightly different values because of the diffusion correction term in the computer program and the assumption that $C^* = 1.0$ ($\rho^*\mu^*/\rho_e\mu_e$) in the theoretical calculations.

The no-blowing values of the Reynolds number based on momentum thickness are shown in Figure 8. This plot shows good agreement with theory for both the laminar and turbulent cases.

5. COOLANT DISTRIBUTION

The computer program is seen to give satisfactorily values for the non blowing Nusselt number, skin friction and momentum thickness. For the blowing case, an overall indication of the results of the methods used can be seen by a comparison of the values from the computer program

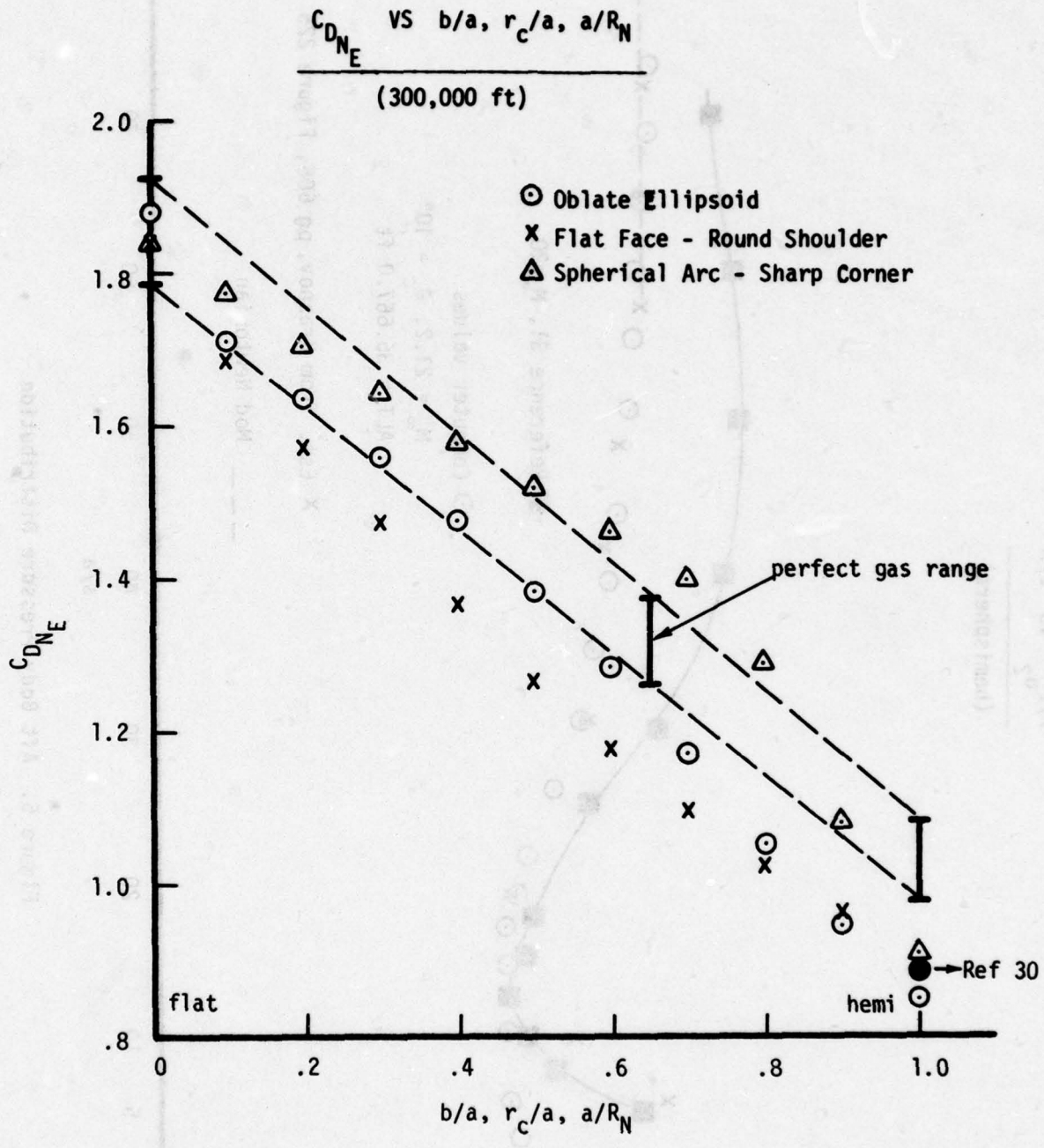

Figure 4. Nose Drag Coefficient Versus Axis Ratio

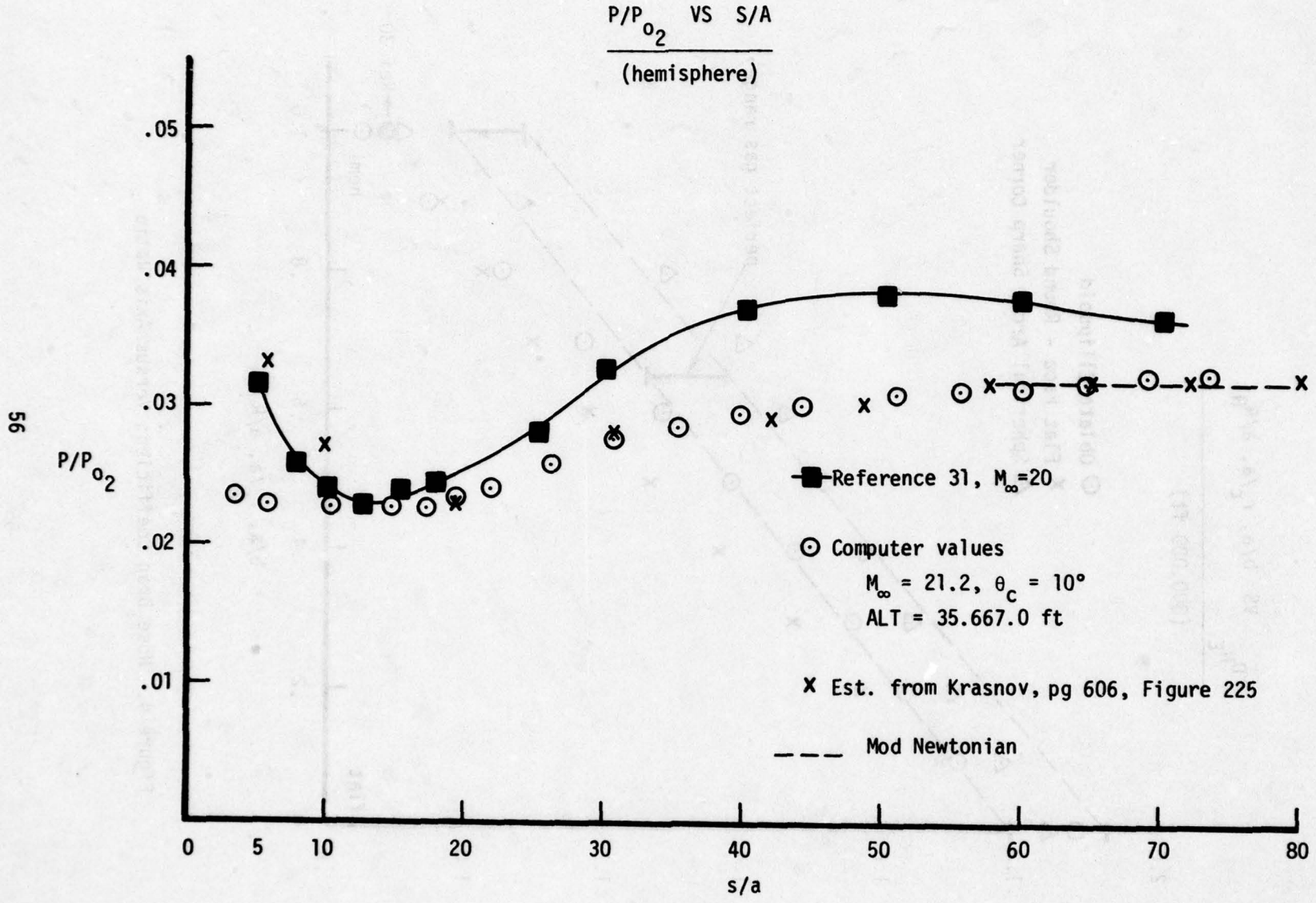

Figure 5. Aft Body Pressure Distribution

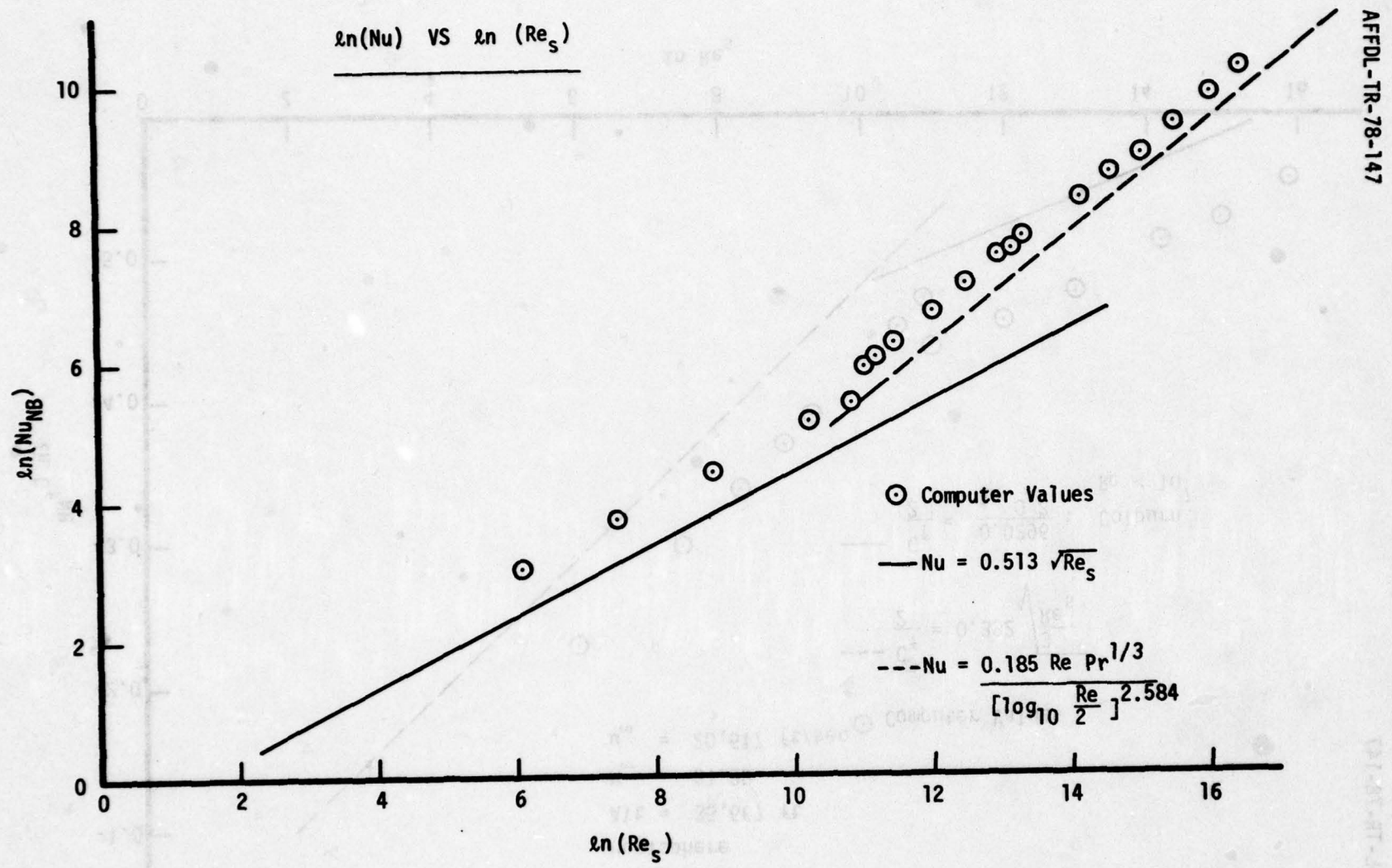

Figure 6. Nusselt Number Versus Reynolds Number (No Blowing)

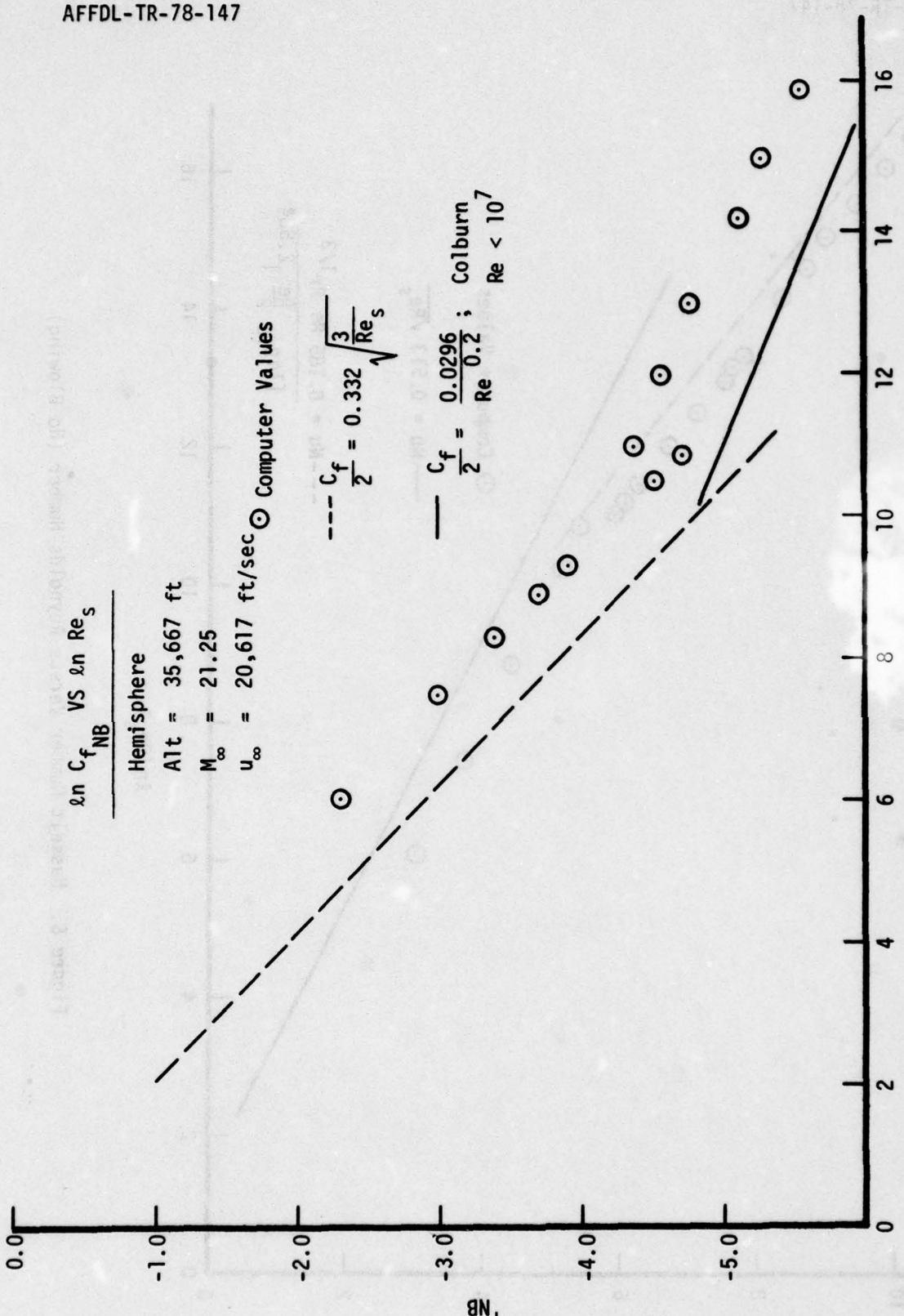

Figure 7. Skin Friction Versus Reynolds Number (No Blowing)

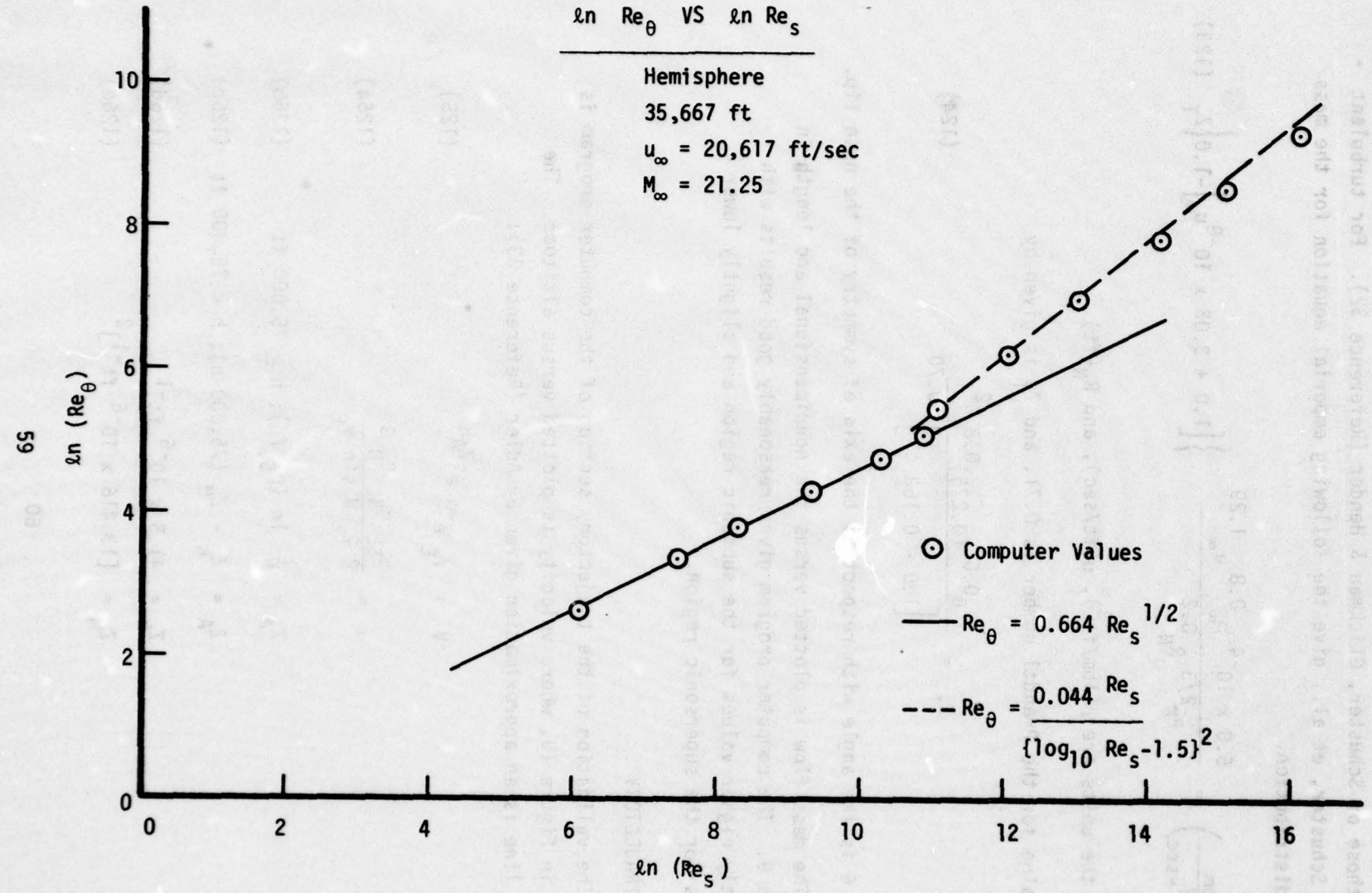

Figure 8. Momentum Thickness Reynolds Number Versus Reynolds Number

with those of Schuster, Glickman & Hender (Reference 32). For turbulent flow, Schuster, et al., give the following emperial equation for the mass flow distribution.

$$\dot{m}\left(\frac{\text{lbm}}{\text{ft}^2\text{-sec}}\right) = \frac{5.0 \times 10^{-4}\ \rho_\infty^{0.8}\ u_\infty^{1.29}}{Pr^{2/3}\ R_N^{0.2}} \left\{\left[1.0 + 3.03 \times 10^{-8} u_\infty\right] - 1.0\right\} Z_T \quad (123)$$

where the units are $\rho(\text{lbm/ft}^3)$, $u(\text{ft/sec})$, and $R_N(\text{ft})$.

The value for the Prandtl number is 0.71, and Z_T is given by

$$Z_T = \frac{\theta^{0.6}\ (0.275)^{0.8}\ \theta^2}{\left[1.0 - 0.168\ \theta^2\right]^{0.70}} \quad (124)$$

where θ is the angle with respect to the axis of symmetry of the nose tip.

The mass flow is plotted versus the nondimensional arc length in Figure 9. The computer program gives reasonably good results with slightly higher values for the subsonic region and slightly lower values for the supersonic region.

6. TRAJECTORY

The validation of the trajectory section of the computer program is shown in Figure 10, where velocity is plotted versus altitude. The solid line is an approximation given by Adler (Reference 33):

$$V = V_E\ e^{-\alpha\ e^{-Z_A h}} \quad (125)$$

where

$$\alpha = \frac{\rho_{SL}\ g_{SL}\ C_D\ S}{2\ Z_k\ W \sin \gamma_E} \quad (126a)$$

$$Z_A = \frac{1}{h}\ \ln\left(\rho_{SL}/\rho\right);\ h \geq 75{,}000 \text{ ft} \quad (126b)$$

$$Z_A = Z_k - Z_M\ (75{,}000\text{-}h);\ h < 75{,}000 \text{ ft} \quad (126c)$$

$$Z_k = 41.5 \times 10^{-6}\ \text{ft}^{-1} \quad (126d)$$

$$Z_M = \left[13.416 \times 10^{-6}\ \text{ft}^{-1}\right]^2 \quad (126e)$$

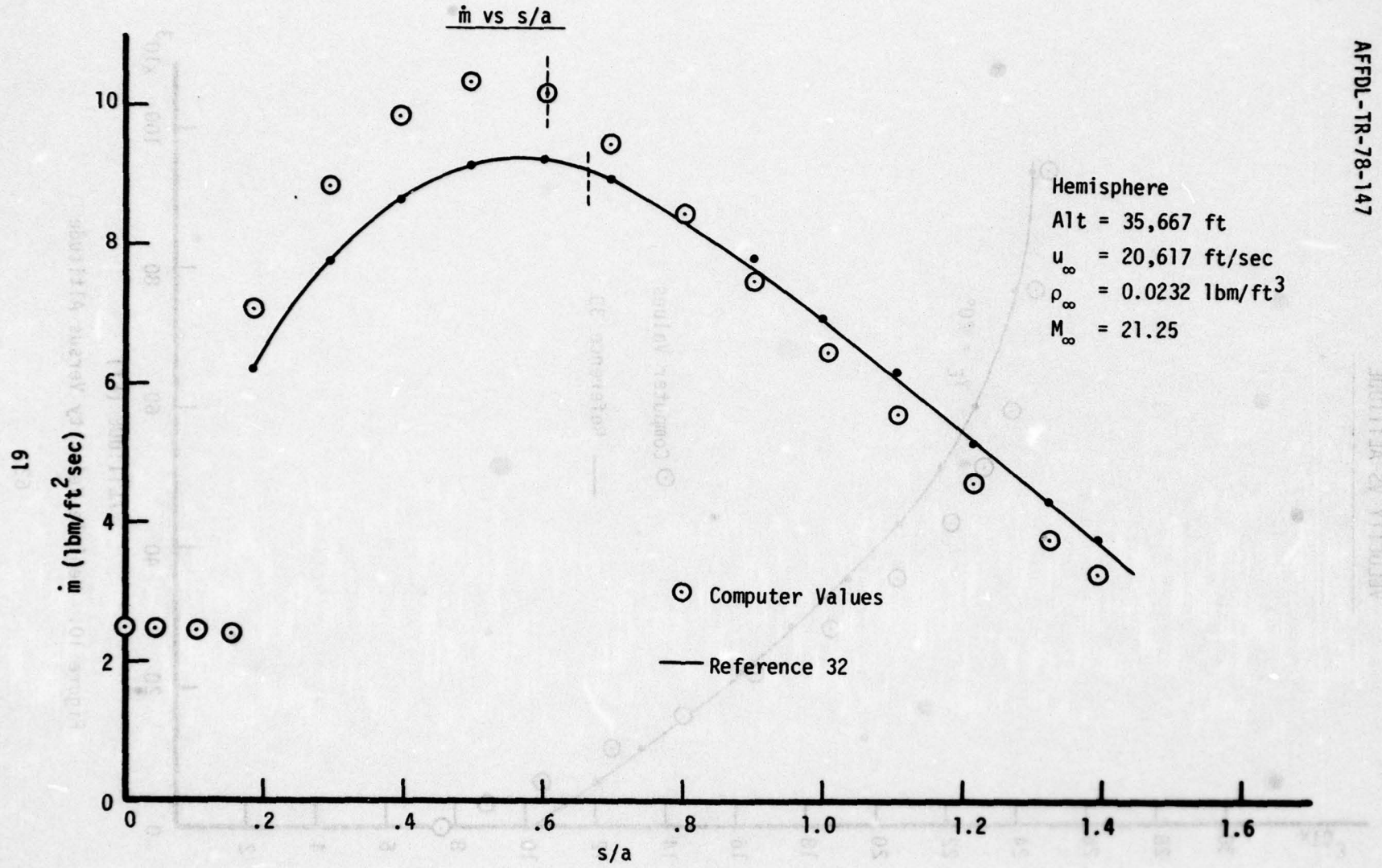

Figure 9. Coolant Distribution Over Hemisphere

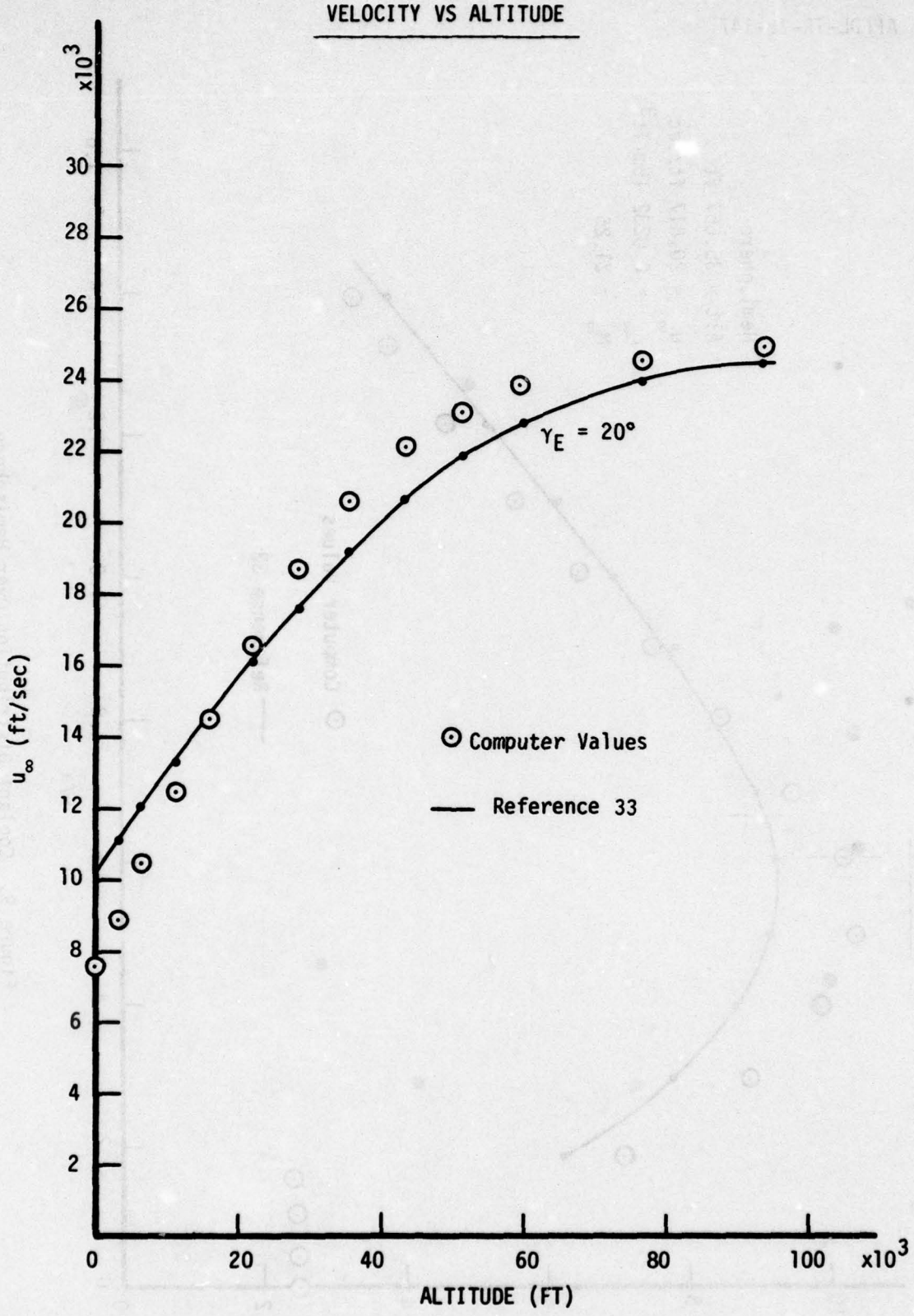

Figure 10. Vehicle Velocity Versus Altitude

The units of ρ are (lb-sec^2/ft^4), g (ft/sec^2), S (ft^2), and WT (lb). The equations assume that α and Z_A are constant, where the computer program allows for quasi variable C_D and γ. Figure 10 shows that the computer program gives reasonable results for the trajectory.

SECTION VII

RESULTS

The results obtained from the investigation are presented in this section. For all of the computer runs the initial reentry conditions were as follows:

Altitude = 300,000 ft
Velocity = 25,000 ft/sec
Trajectory Angle = -20 deg

The three different nose shapes were first run with the following vehicle conditions:

Nose base radius (a) = 1.0 inch
Length = 72.0 inch
Cone half angle = 10 deg
Weight = 800 lb

1. NOSE SHAPE EFFECT ON COOLANT

The nose bluntness of the different noses was varied by changing the minor axis value (b) for the oblate nose, the shoulder radius (r_c) for the flat face nose, and the nose radius (R_N) for the spherical arc nose. The results obtained are plotted in Figure 11, which shows the coolant required for the trajectory versus the nose bluntness parameters, b/a, r_c/a, or a/R_N. The spherical arc family is seen to be the best of the families considered and the flat face - sharp corner is the best shape, requiring only about 40% of the amount of coolant of the hemisphere. The flat face requires less coolant because of both the smaller area and lower overall heat loading of the flat face as compared to the hemisphere. The flat face surface area is one half of the surface area of a hemisphere. The heat flux at the maximum heating conditions for the flat face and hemisphere is plotted in Figure 12. This figure shows that the flat face has a lower stagnation point heating, that transition occurs later for the flat face, and that the maximum heating is smaller for the flat face. Thus the intensity of the heating for the flat face is not only lower but also occurs over a smaller area.

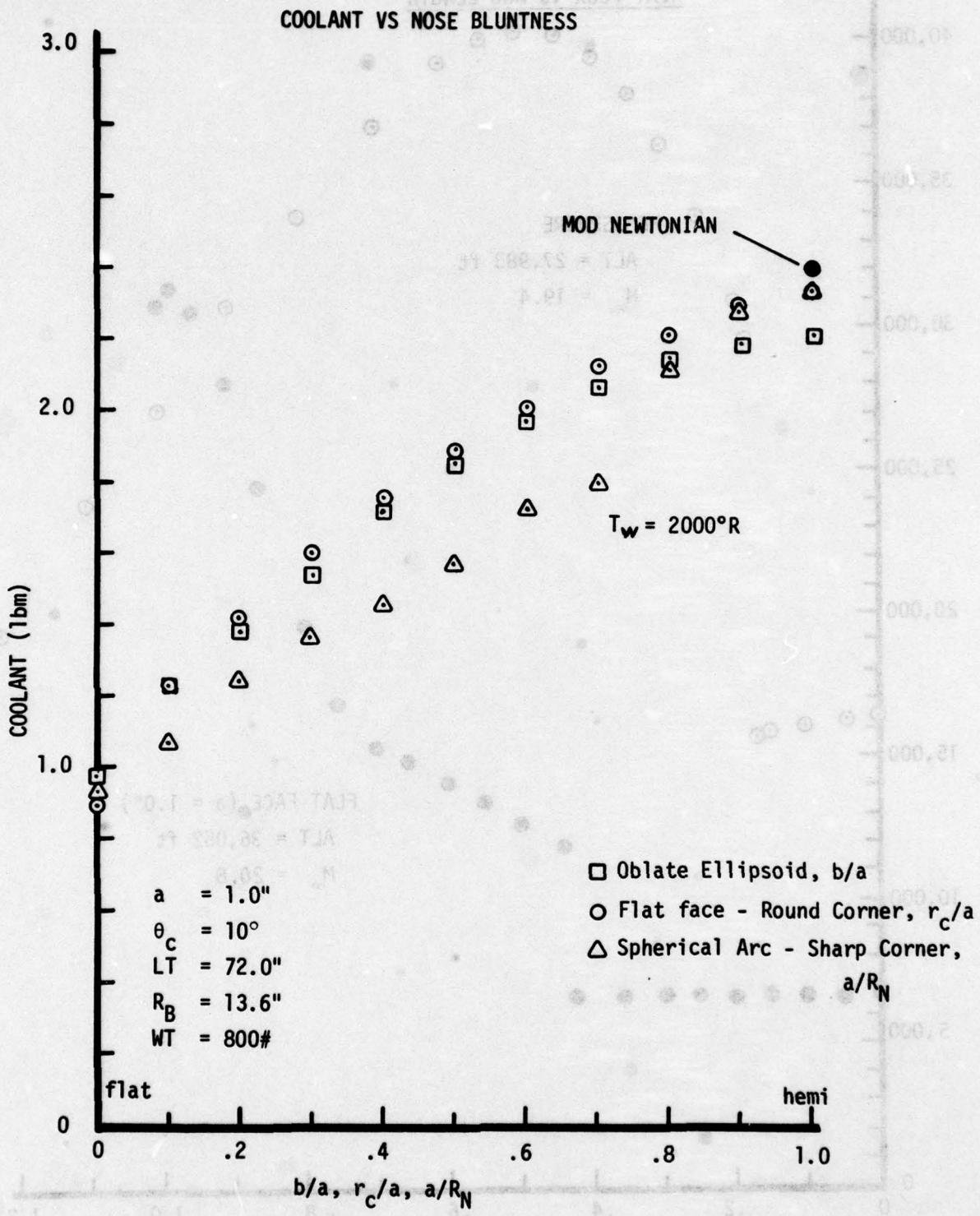

Figure 11. Coolant Amount Versus Nose Axis Ratio

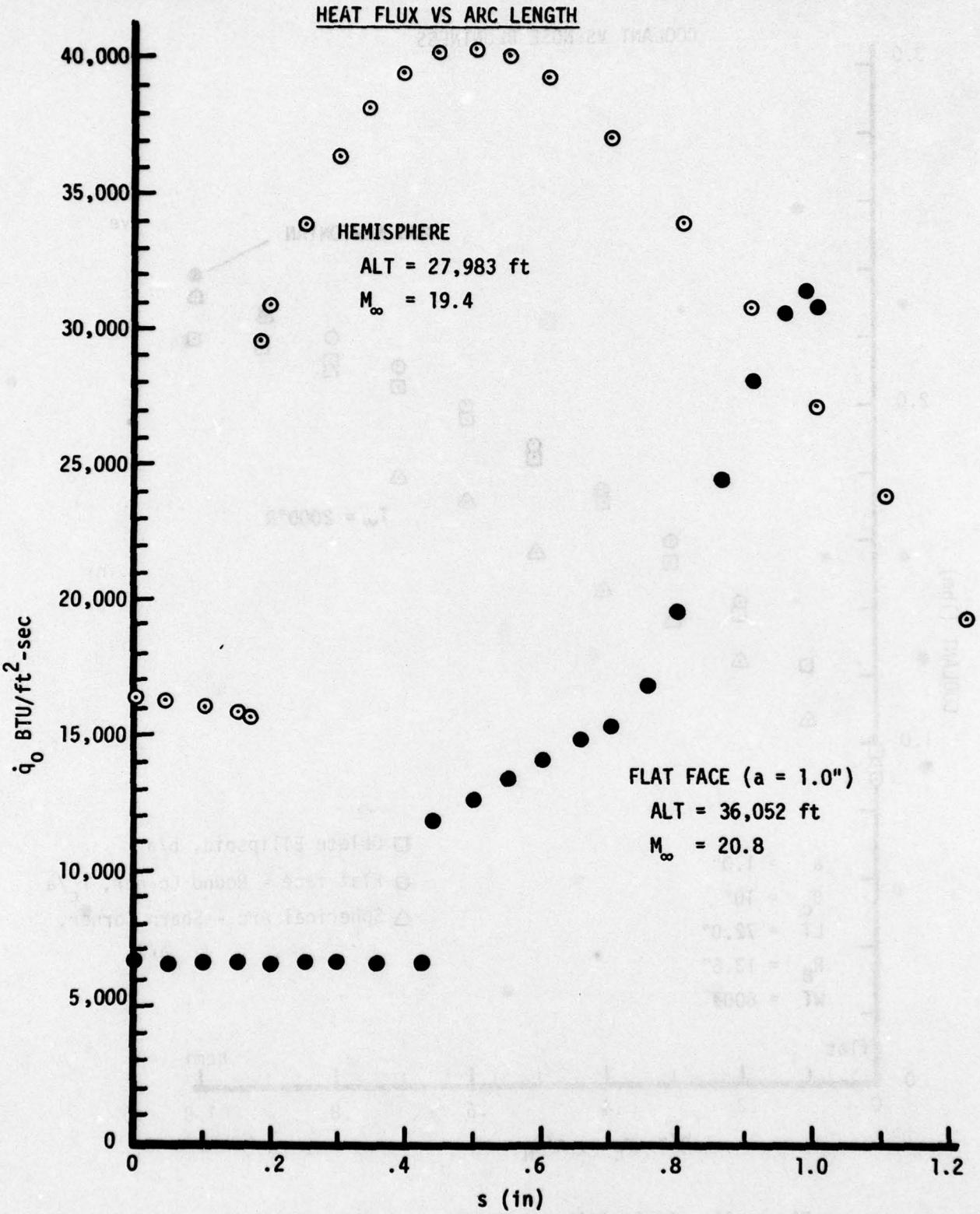

Figure 12. Heat Flux Distribution for Hemisphere and Flat Face at Maximum Heating Altitude

As mentioned, Figure 11 shows that the spherical arc - sharp corner nose shapes require less coolant for bluntness parameters less than 0.70. This is also due to the smaller area and heat loading of the spherical arc nose shape as compared to the flat face - round shoulder or oblate ellipsoid shapes. The surface area for the three different nose shapes are plotted in Figure 13, where the spherical arc shape is seen to have the least area for a given axis ratio. The flat face - round shoulder has the most area for a given axis ratio. This corresponds to the coolant requirements shown in Figure 11. The heat flux at the maximum heating conditions for an axis ratio of 0.70 is plotted in Figure 14. Even though the spherical arc nose has a slightly higher stagnation point heating, the overall heating intensity is lower and occurs over a smaller area.

For values of a/R_N greater than 0.70, Figure 11 shows the coolant required for the spherical arc noses to be the same as the other two noses. The "jump" at $a/R_N = 0.70$ is due to the "jump" in the sonic point location. For $a/R_N \leq 0.7$ ($\theta_J \geq 45°$), the sonic point is assumed to be at the corner. For $a/R_N > 0.70$ ($\theta_J < 45°$), the sonic point location moves toward the hemispherical value. As turbulent, subsonic flow has associated with it higher heating rates, the nose shape that has the sonic point further downstream will require less cooling.

2. NOSE SHAPE EFFECT ON TRAJECTORY

The time to impact for the data plotted in Figure 11 varied from 37.5 to 38.8 seconds. Practically speaking then, the time to impact is the same for all of the nose shapes because the nose drag was small compared to the total drag of the vehicle, 7% for the hemisphere and 11% for the flat face. In order to determine the effect of the nose shape on the trajectory as well as the coolant required, the program was rerun for the oblate ellipsoid family with larger nose base radii. The vehicle parameters were as follows:

a =	2.0"	3.0"
L =	72.0"	72.0"
θ_c =	9.23°	8.45°
R_B =	13.7"	13.7"
WT =	1200 lb	1200 lb

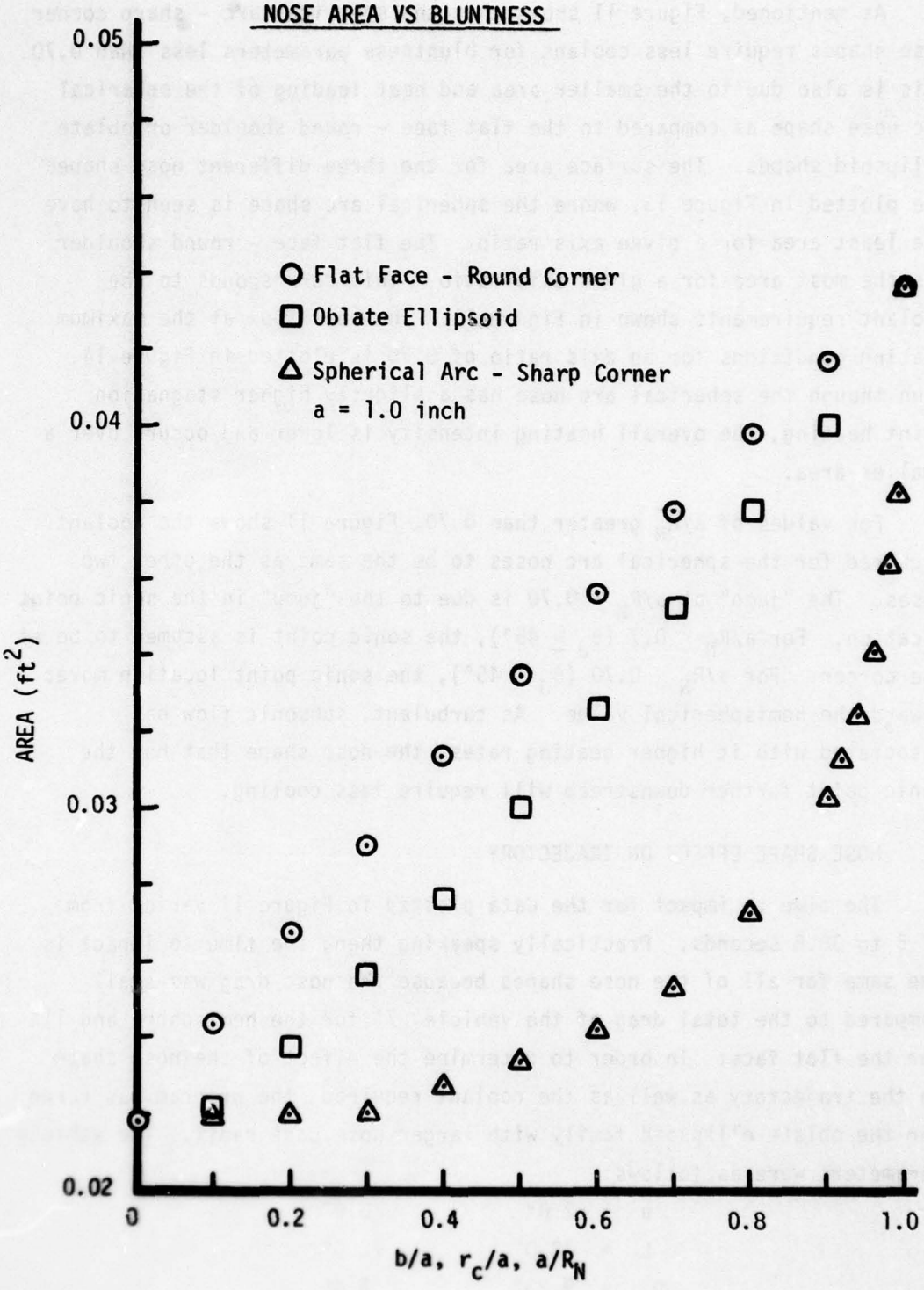

Figure 13. Nose Surface Area Versus Axis Ratio

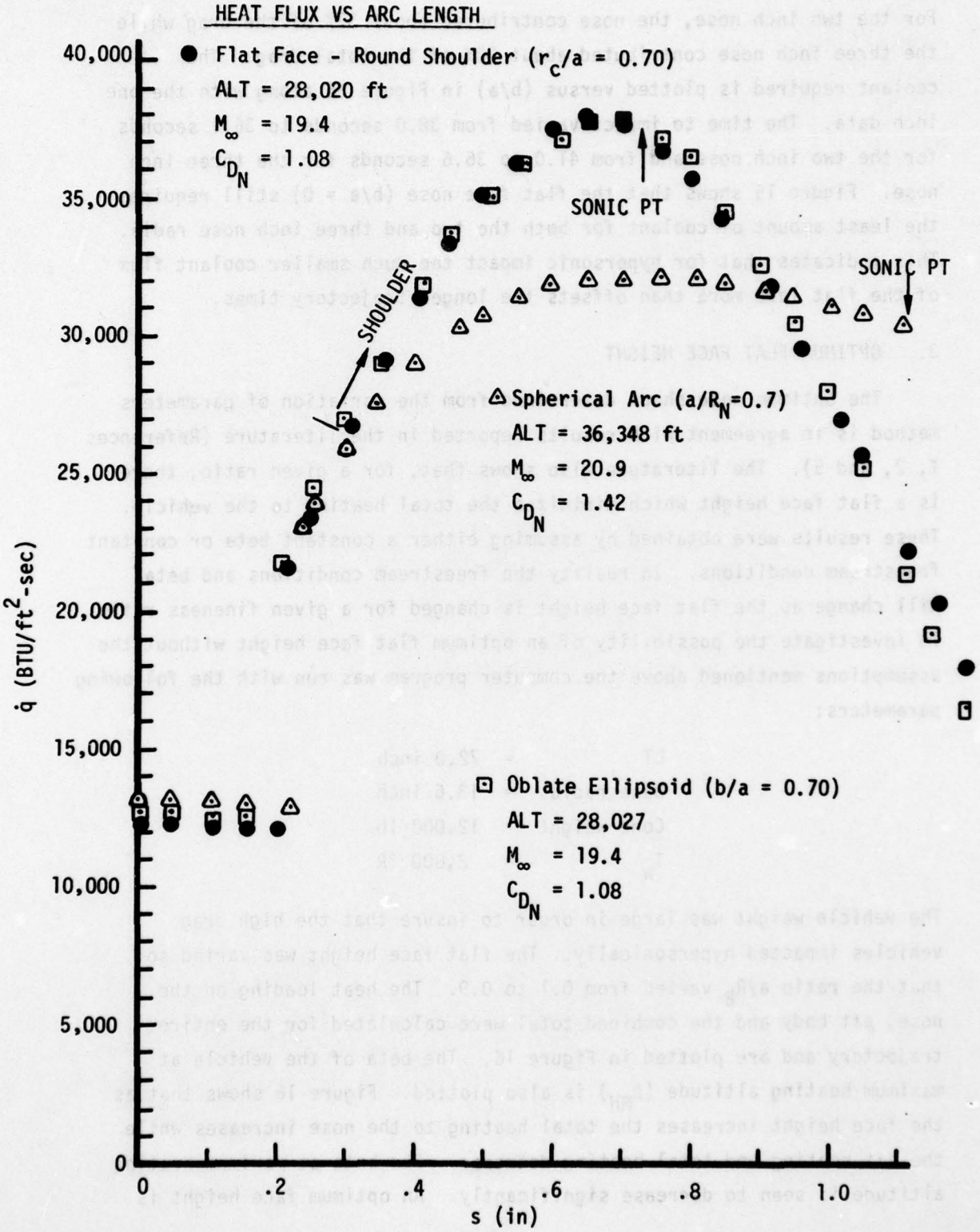

Figure 14. Heat Flux Distribution for Nose Axis Ratio of 0.70

For the two inch nose, the nose contributed about 37% of the drag while the three inch nose contributed about 50% of the total drag. The coolant required is plotted versus (b/a) in Figure 15 along with the one inch data. The time to impact varied from 38.0 seconds to 36.1 seconds for the two inch nose and from 41.0 to 36.6 seconds for the three inch nose. Figure 15 shows that the flat face nose (b/a = 0) still requires the least amount of coolant for both the two and three inch nose radii. This indicates that for hypersonic impact the much smaller coolant flux of the flat face more than offsets the longer trajectory times.

3. OPTIMUM FLAT FACE HEIGHT

The optimum nose shape determined from the variation of parameters method is in agreement with results reported in the literature (References 1, 2, and 5). The literature also shows that, for a given ratio, there is a flat face height which minimizes the total heating to the vehicle. These results were obtained by assuming either a constant beta or constant freestream conditions. In reality the freestream conditions and beta will change as the flat face height is changed for a given fineness ratio. To investigate the possibility of an optimum flat face height without the assumptions mentioned above the computer program was run with the following parameters:

LT	=	72.0 inch
Base radius	=	13.6 inch
Cone weight	=	12,000 lb
T_w	=	2,000 °R

The vehicle weight was large in order to insure that the high drag vehicles impacted hypersonically. The flat face height was varied so that the ratio a/R_B varied from 0.1 to 0.9. The heat loading on the nose, aft body and the combined total were calculated for the entire trajectory and are plotted in Figure 16. The beta of the vehicle at maximum heating altitude (β_{MH}) is also plotted. Figure 16 shows that as the face height increases the total heating to the nose increases while the aft heating and total heating decrease. The beta at maximum heating altitude is seen to decrease significantly. An optimum face height is

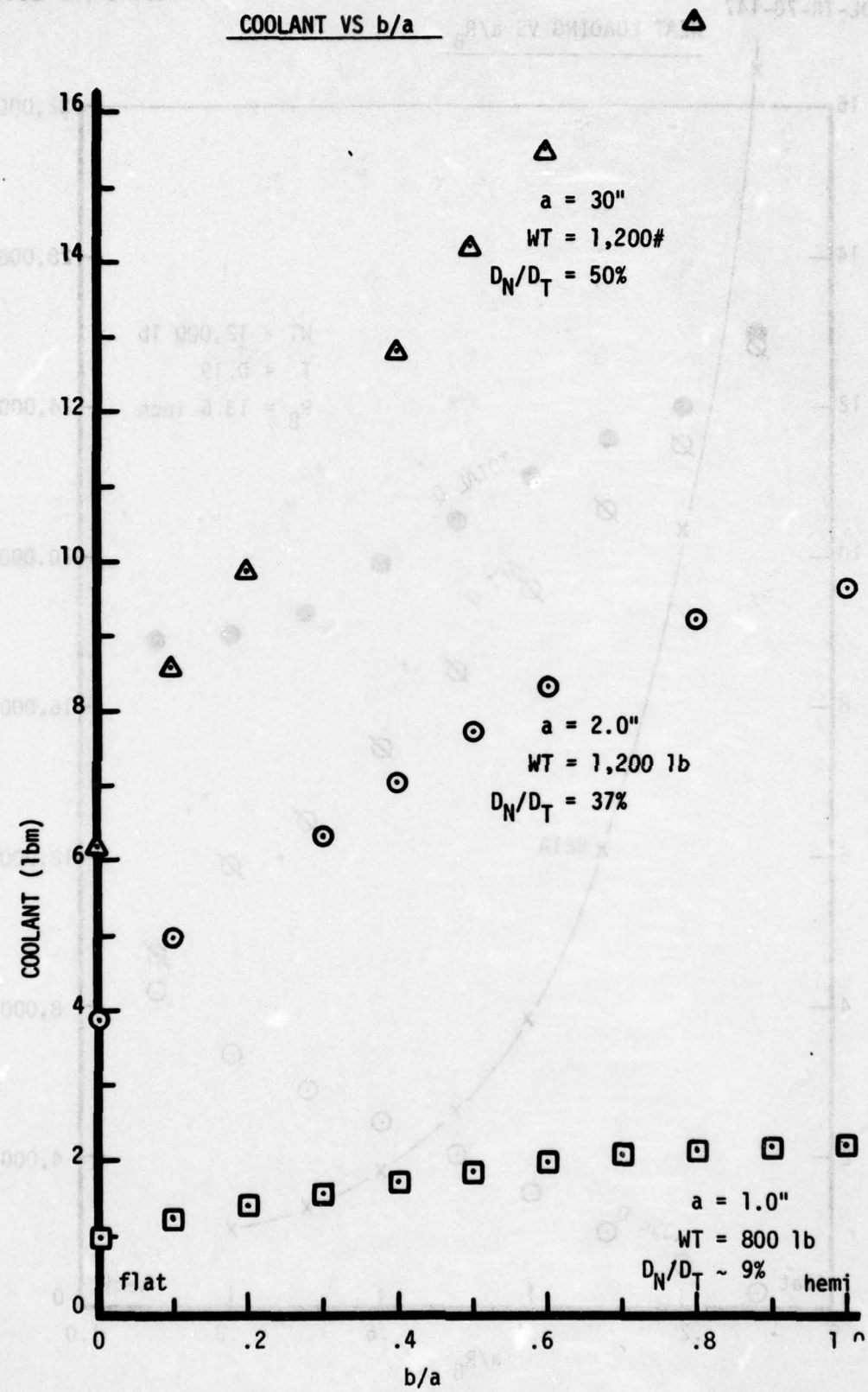

Figure 15. Total Coolant Required for Different Size Nosetips

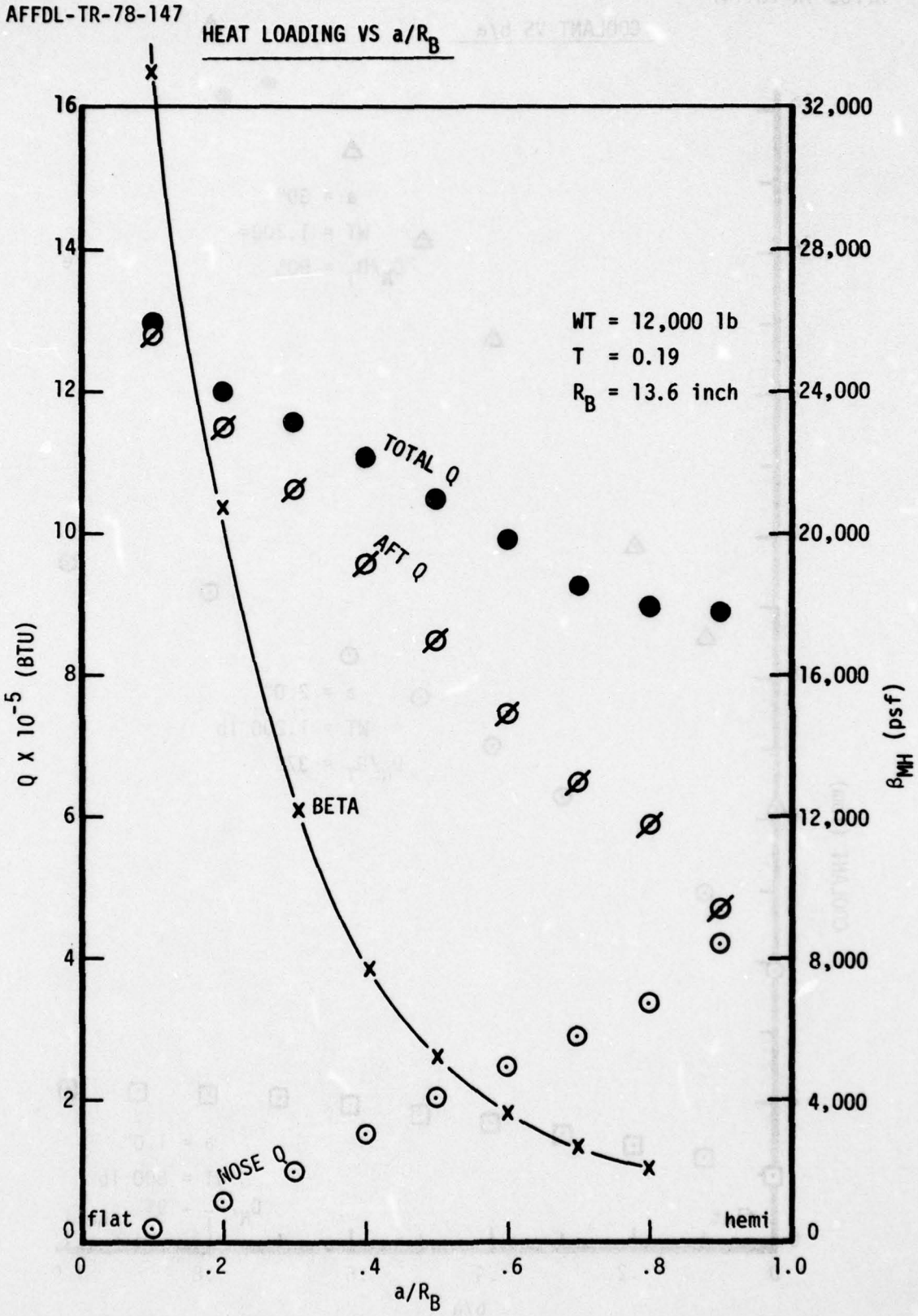

Figure 16. Heat Loading on Vehicle for Vehicle of Constant Weight (b/a=0.0)

not observed. As the flat face height increases, the drag of the vehicle increases causing the velocity and hence heating intensity to decrease. The decrease in heating intensity over the vehicle more than offsets the increase to the nose because of a larger nose area. The total coolant required for the varying face heights is shown in Figure 17. As can be seen, the coolant required increases drastically as the flat face heights is increased.

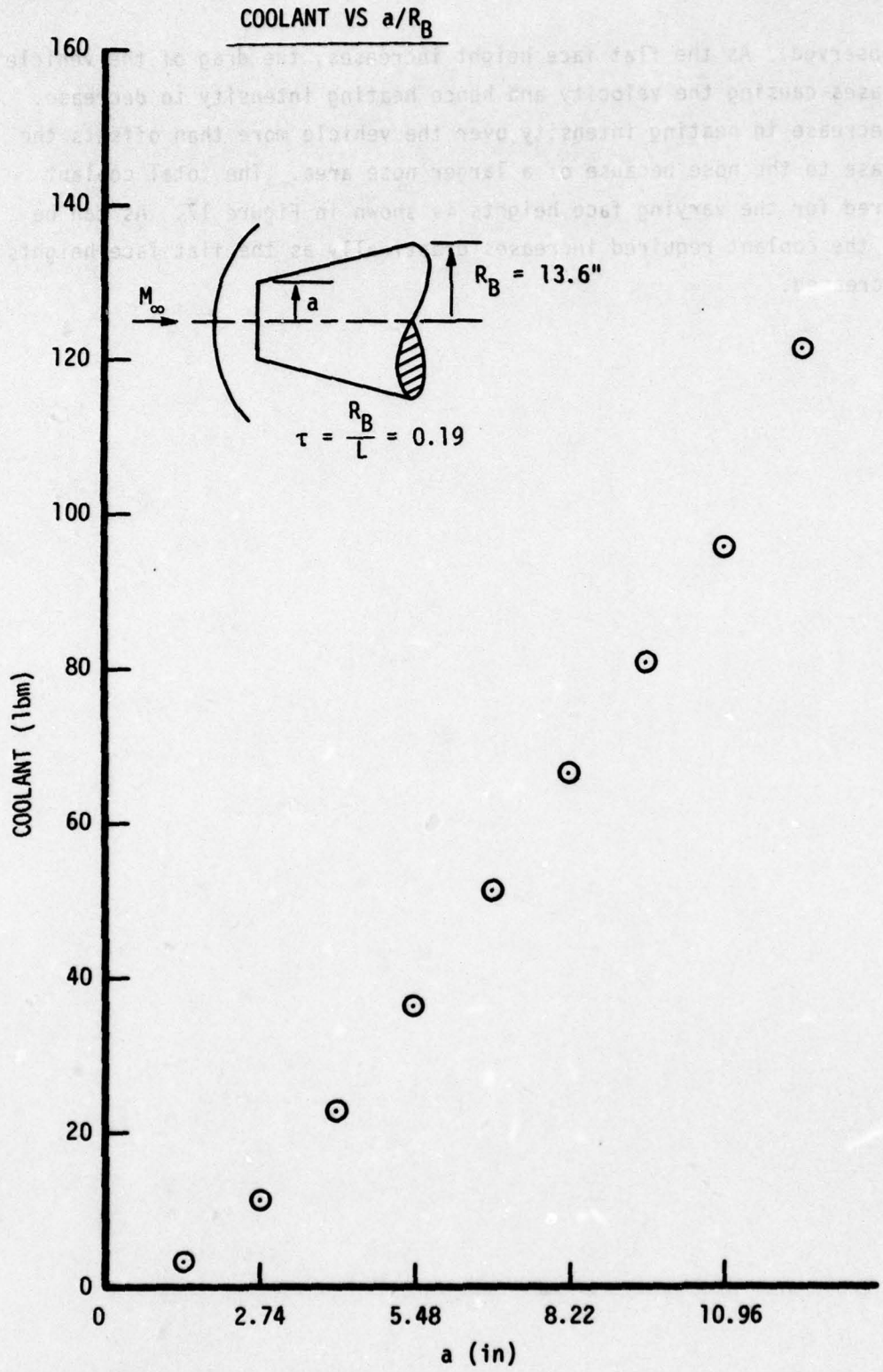

Figure 17. Total Coolant Required for Different Flat Face Heights

SECTION VIII

CONCLUSIONS

The results of this investigation can be summarized as follows. For reentry vehicles impacting hypersonically the flat face - sharp corner nose is the optimum TCNT shape. This was found to be true for nose sizes that contributed up to 50% of the total drag of the vehicle. Using a flat face nose shape reduces the amount of water needed, and hence volume, about 60%. This is about one pound savings in weight for a one inch nose radius and 5.5 pound saving for the two inch nose radius. No flat face height was found that minimized the total heating to the entire reentry vehicle for any of the nose radii considered. If the fineness ratio and weight of the vehicle are fixed, the overall heating decreases as the flat face height increases due to the resulting large decrease in the velocity of the vehicle.

The effect of the nose shape on the trajectory depends on the size of the nose. For low drag noses, 7 - 10% of total drag, the nose shape has very little effect on trajectory times. As the nose drag increases to 50% of the total drag, the flat face trajectory time is about 12% greater than that for a hemisphere.

Practically speaking it may not be possible to provide enough coolant at the corner of the flat face. A rounding of the corner will then be necessary. If the corner can be adequately cooled for round shoulders with r_c less than or equal to 0.2a, the flat face - round shoulder shape is the optimum shape. If r_c is greater than 0.2a, then the oblate ellipsoid shape is the better shape.

REFERENCES

1. Aihara, Y., "Optimum Body Geometries of Minimum Heat Transfer at Hypersonic Speeds," AIAA Journal, Technical Notes, Vol. 6 No. 11, November 1968, pp. 2187 - 2188.

2. Crowell, P. G., Optimum Nosetip Geometries for Aerodynamic Heating - Specified Fineness Ratio, The Aerospace Corporation, Interoffice Correspondence, No. 73-5134.5-001, January 1973.

3. Furey, R. J., Optimum Super/Hypersonic Leading - Edge Profiles, David Taylor Model Basin Report 2035, July 1965.

4. Perminov, V. D., and Solodkin, Ye., Ye., "Minimum-Drag Bodies with Minimum Heat Flux to the Surface with Laminar and Turbulent Boundary-Layer Flows," Heat Transfer - Soviet Research, Vol. 4 No. 2, March-April 1972, pp. 137-145.

5. Baker, R. L., and Kramer, R. F., Nosetip Shape Optimization for Minimum Transpiration Coolant Requirements, Paper 77-780 AIAA 12th Thermophysics Conference, Albuquerque, N. Mex., June 27-29, 1977.

6. Hull, D. G., "On Hypersonic Shapes of Minimum Heat Transfer," The Journal of the Astronautical Sciences, Vol. XVII, No. 1, July-Aug 1969, pp. 60-62.

7. Dommasch, D. O., Sherby, S. S., and Connolly, T.F., Airplane Aerodynamics, Fourth Edition, Pitman Publishing Comp., N.Y., 1967.

8. Hansen, C. F., Approximations for the Thermodynamic and Transport Properties of High Temperature Air, NACA TN-4150, March 1958.

9. Krasnov, N. F., Aerodynamics of Bodies of Revolution, American Elseirer Publishing Company, Inc., New York, 1970.

10. James, C. S., and Terry, J. E., "Shock-Wave Profiles Over Ellipsoidal Nosed Bodies in Hypersonic Flow," Journal Aerospace Sciences, Vol. 29, No. 9, Sept. 1962, pp. 1128-1129.

11. Felderman, E. J., and Fallinger, R. C., "Stagnation-Point Heat Transfer and Shock - Detachment Distance for Ellipsoids of Revolution," AIAA Journ., Vol. 3, No. 6, June 1965, pp. 1207-1208.

12. Vinokur, M., "Laminar Heat - Transfer Distribution on Oblate Ellipsoidal Noses in Hypersonic Flow," Journ. of the Aero/Space Sciences, Vol. 29, No. 1, Jan. 1962, pp. 113-114.

13. Vinokur, M., "Hypersonic Flow Around Bodies of Revolution which are Generated by Cone Sections," Proceedings of the Sixth Midwestern Conference on Fluid Mechanics, Univ. of Texas, September 1959, pp. 232-253.

REFERENCES (CONTINUED)

14. Vinokur, M., "Inviscid Hypersonic Flow Near the Stagnation Point of Oblate Ellipsoids Noses," Journ. of the Aero/Space Sciences, Vol. 25, No. 7, July 1958, pg. 468.

15. Yelmgren, K. E., Simplified Method for Calculating the Hypersonic Pressure Distribution about Blunt Oblate Ellipsoids, AFFDL-TM-76-112-FXE, October 1976.

16. Pappas, C. C. and Lee, G., "Heat Transfer and Pressure on a Hypersonic Blunt Cone with Mass Addition," AIAA Journ, Vol. 8, No. 5, May 1970, pp. 954-956.

17. Boison, J. C., and Curtiss, H. A., "An Experimental Investigation of Blunt Body Stagnation Point Velocity Gradient," ARS Journal, Vol. 29, No. 2, Feb 1959, pp. 130-135.

18. Hansen, C. J., and Heims, S. P., A Review of the Thermodynamic, Transport and Chemical Reaction Rate Properties of High Temperature Air, NACA TN-4359, July 1958.

19. Bade, W. L., "Simple Analytical Approximations to the Equations of State of Dissociated Air," ARS Journal, Vol. 29, No. 4, April 1959, pp. 298-299.

20. Eckert, E. R. G., Survey of Boundary Layer Heat Transfer at High Velocities and High Temperatures, WADC TR-59-624, April 1960.

21. Fox, H., and Libby, P. A., "Helium Injection into the Boundary Layer at an Axisymmetric Stagnation Point," Journ. of Aero/Space Sciences, Vol. 29, No. 8, August 1962, pp. 921-934.

22. Lees, L., "Laminar Heat Transfer Over Blunt-Nosed Bodies at Hypersonic Flight Speeds," Jet Propulsion, April 1959, pp. 259-274.

23. Langanelli, A. L., Fogaroli, R. P., and Martellucci, A., The Effects of Mass Transfer and Angle of Attack on Hypersonic Turbulent Boundary Layer Characteristics, AFFDL-TR-75-35, April 1975.

24. Timmer, H. G., Arne, C. L., Stokes, T. R., and Tang, H. H., Ablation Methods for Slender Reentry Bodies, AFFDL-TR-70-27, Vol I, March 1970.

25. Gold, H., Surface Fluid and Boundary Layer Interaction Aspects of Transpiration - Cooled Nosetip Concepts, AFML-TR-73-8 May 1973.

26. Van Driest, E. R., "On the Aerodynamic Heating of Blunt Bodies," Z. Agnew. Math. Phip., Vol. IX b, 1958, pp. 233-248.

REFERENCES (CONCLUDED)

27. Cresci, R. J., MacKenzie, D. A., and Libby, P. A., "An Investigation of Laminar, Transitional, and Turbulent Heat Transfer on Blunt-Nosed Bodies in Hypersonic Flow," Journ. Aero/Space Sciences, Vol. 27, No. 6, June 1960, pp. 401-414.

28. Hoerner, S. F., Fluid-Dynamic Drag, Published by the Author, 1965.

29. Carnahan, B., Luther, H. A., and Wilkes, J. O., Applied Numerical Methods, John Wiley and Son, Inc., New York, 1969.

30. Gregorek, G. M., and Korkan, K. P., Hypersonic Blunt Body Similtude in a Perfect Gas, AFFDL-TDR-64-92, June 1964.

31. Roberts, J. F., Lewis, C. H., and Reed, M., Ideal Gas Spherically Blunted Cone Flow Field Solutions at Hypersonic Conditions, AEDC-TR-66-121, August 1966.

32. Schuster, J. R., Glickman, R. A., and Hender, D. R., "Transpiration Nosetip Coolant Flow Control," Journ. Spacecraft and Rockets, Vol. 11, No. 3, March 1974, pp. 152-158.

33. Adler, A. A., "Calculation of Reentry Velocity Profile," Jet Propulsion, Vol. 28, No. 12, Dec. 1958, pp. 827-828.

34. Zoby, E. V., and Sullivian, E. M., Effects of Corner Radius on Stagnation-Point Velocity Gradients on Blunt Axisymmetric Bodies, NASA TM-X-1067, March 1965.

*U.S.Government Printing Office: 1979 — 657-002/15